UCRL-ID-135740

High Precision Droplet Based Net-Form Manufacturing

A.B. Shapiro

September 16, 1999

U.S. Department of Energy

Lawrence
Livermore
National
Laboratory

High Precision Droplet Based Net-Form Manufacturing

LDRD Project 98-ERD-085

Arthur B. Shapiro
New Technologies Engineering Division
Mechanical Engineering

September 1999

This document is a compilation of reports by the following people who worked on this LDRD project.

Section	Title	Author
1	Introduction and Overview	Arthur B. Shapiro Melissa Orme (UC Irvine)
2	HOTDROP Operation Guidelines UCRL-CODE-99040	Wayne O. Miller
3	Spray Deposition Modeling with ALE3D	Vivek Sahai
4	Estimating the Maximum Splat Diameter of a Solidifying Droplet	Nicolas Hadjiconstantinou
5	An Accuracy Evaluation for the Madejski Splat Quench Solidification Model, UCRL-JC-133757	Salvador Aceves
6	Droplet Drag and heat Transfer During Time Of Flight	Salvador Aceves

Engineering LDRD-ER

Project 98-ERD-085

High Precision Droplet Based Net-Form Manufacturing

PI: Arthur B. Shapiro
Melissa Orme (University of California, Irvine)

In collaboration with the University of California at Irvine (UCI), we are working on a new technology that relies on the precise deposition of nanoliter molten-metal droplets that are targeted onto a substrate by electrostatic charging and deflection. By this way, three-dimensional (3D) structural materials can be manufactured microlayer by microlayer. Because the volume of the droplets are small, they rapidly solidify on impact, bringing forth a material component with fine grain structures which lead to enhanced material properties (e.g., strength). UCI is responsible for an experimental investigation of the manufacturing feasibility of this process. LLNL has unique expertise in the computational modeling of 3D heat transfer and solid mechanics and has the large-scale computer resources necessary to model this large system. Process modeling will help move this technology from the bench-top to an industrial process. Applications at LLNL include rapid prototyping of metal parts and manufacturing new alloys by co-jetting different metals.

Motivation

This new manufacturing process has the potential to fabricate parts with greater strength, using novel alloys, and shapes than can be done today. The very rapid solidification of nano-liter sized metal droplets leads to finer grains which results in a part possessing higher strength than achievable by conventional casting processes. New and novel alloys can be created by co-jetting droplet streams using different metals of different droplet size and deposition rates. Additionally, the microstructure can be varied at different locations in the fabricated part by our ability to control the droplet size, deposition rate, and temperature.

Using multiple nozzles with droplet deposition rates of 40,000 droplets/second would provide a means for rapid prototyping metal parts. Currently, there are several manufacturing techniques for rapid prototyping parts using plastic. However, no adequate methods exist for rapid prototyping parts using metal. This capability would benefit LLNL's design engineers building one-of-a-kind metal parts or small production quantities.

This new "micro-casting" process for manufacturing parts with finer grain structures and geometric fidelity may be a viable alternative to the conventional casting of special nuclear materials. An additional application would be the manufacturing of hybrid MEMS devices; such as, fabricating a three dimensional metal structure on an etched MEMS device.

Accomplishments 5/98 – 9/99

Figure 1 is a schematic of the droplet manufacturing facility at UCI. A crucible at the top of the apparatus contains liquid metal which flows through an orifice forming a capillary stream into the lower vacuum chamber. A method for generating deterministic droplet patterns from capillary stream breakup has been developed by Orme. By applying specific amplitude-modulated disturbances with an arbitrary modulation to a viscous capillary stream, predictable

and flexibly controlled patterns of droplets can be obtained. The disturbance is created by a piezo-electric transducer above the orifice. The metal droplets are charged and their trajectory is controlled by deflection electrodes. The substrate itself can be moved by a controllable x-y positioning table for fabricating planar 3-dimensional parts, or the substrate rotated to fabricate axisymmetric parts as shown in Figure 2. The parts in Figure 2 were fabricated from a former prototype facility using 200 μm solder droplets. The scope of this work is to push the technology so that higher melting point metals can be used (e.g., aluminum) and smaller droplet sizes can be formed (e.g., 5 - 50 μm) to fabricate thin walled parts of interest to LLNL.

Figure 1: This schematic depicts the High Precision Droplet-Based Net-Shape Manufacturing facility at UCI.

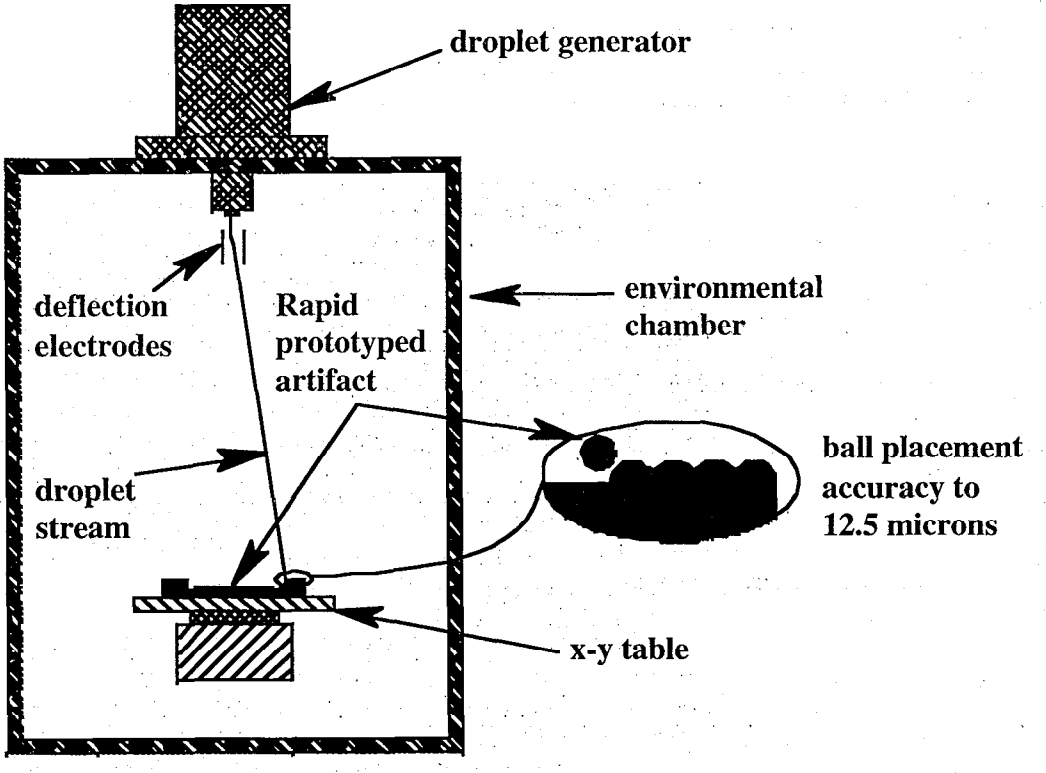

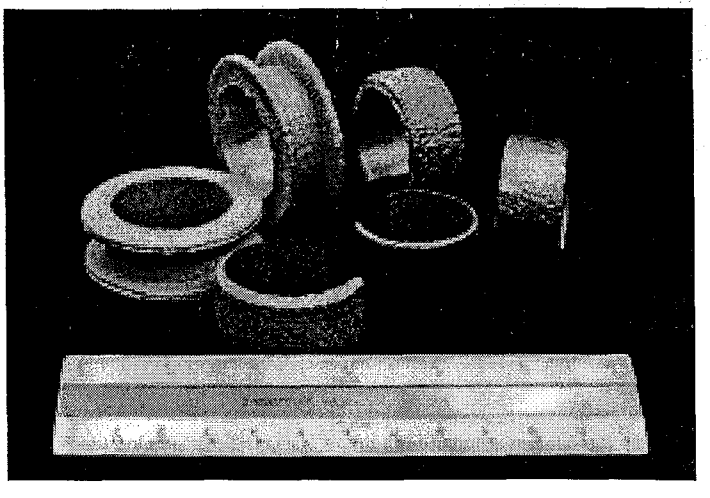

Figure 2: These axisymmetric parts were fabricated from a prototype facility using 200 μm solder droplets. The scope of this work is to push the technology so that higher melting point metals can be used (e.g., aluminum) and smaller droplet sizes can be formed (e.g., 5 - 50 μm) to fabricate thin walled parts of interest to LLNL.

During 1998, UCI began moving the technology forward from solder droplets to more interesting materials with higher melting points, such as aluminum. A new facility came on-line in August 1998. By the end of the year, metallurgical investigations of sectioned aluminum-droplet-on-substrate samples from initial shake-down runs had revealed that the grain structure was equiaxed, the grain size ranged from 120 to 150 μm, the average porosity was about 3%, and oxides and other impurities were present. Tensile tests were promising: the measured yield stresses (8900 psi) were greater than both the yield stress for the starting aluminum ingot (6816 psi) and published handbook values for aluminum (6800 psi).

A significant fabrication challenge this year was to overcome the inclusion of oxides and other contaminants in the droplet stream, which would result in defective parts. Figure 3 shows a droplet formed "stalagmite" (on the right) with a significant presence of oxides indicated by the dark mottled exterior. A filter pack was designed to fit at the bottom of the liquid metal crucible. After four design iterations, we successfully filtered the metal stream and reduced the oxides as shown by the shiny stalagmite on the left in Figure 3.

Figure 3: These aluminum stalagmites were fabricated by directing a stream of aluminum droplets downward onto a substrate. The stalagmite on the right shows the presence of oxides indicated by the dark mottled exterior. A significant challenge was to design a filter to reduce the oxides and other contaminants. This was successfully accomplished as demonstrated by the shiny stalagmite on the left.

During the shake-down runs, we also noted a loss of control on the deposited location of the droplets. This was caused by electrostatic interaction between the closely spaced charged droplets. The solution was to charge alternate droplets in the stream and capture the uncharged droplets following a straight trajectory by a "gutter" to prevent them from striking the substrate. The charged droplets, with a curved trajectory, avoid capture by the gutter. We seem to have gotten the operating procedure down for creating a uniform stream of droplets. We are concentrating now on making components. We have made three cylinders from three different runs but haven't honed in on the correct temperature or speed conditions yet. We have some

really porous or really "globby" cylinders depending on our conditions. The poor quality of these cylinders are good illustrations of the need for precise operating conditions and show the critical importance of the modeling effort to guide the experiments.

During the last year, LLNL pursued process modeling both on the micro-scale of an individual droplet striking a substrate and on the larger system scale to predict velocity and temperature drop during time of flight. We also investigated material constitutive models that would capture the low strength of the metal in the liquid state and transition to the higher strength solid.

Empirical equations were found in the literature to predict the temperature and velocity drop during time of flight. These equations also include the effect of the wake of one droplet on a trailing droplet. Figure 4 shows the temperature drop of a 189 μm aluminum droplet with an initial velocity of 9 m/s in nitrogen as a function of chamber pressure. The bottom curve shows that a droplet with an initial temperature of 1200K will solidify before striking the substrate at chamber pressures above 40 kPa. Such curves helped define the process parameters of crucible temperature and chamber pressure that would result in a liquid droplet with a specified superheat when striking the substrate.

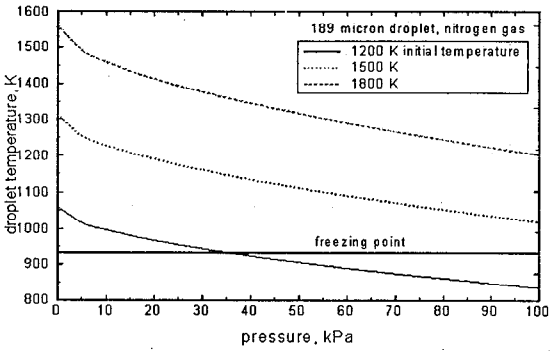

Figure 4: Shown is the temperature drop of a 189 μm aluminum droplet with an initial velocity of 9 m/s in nitrogen as a function of chamber pressure. Such curves helped define the process parameters of crucible temperature and chamber pressure that would result in a liquid droplet with a specified superheat when striking the substrate.

Our next step is to incorporate these empirical equations into our finite element heat transfer code TOPAZ. This will allow us to do system process modeling. Our approach is to "birth" finite elements (but without modeling the impact process – see next paragraph) at the droplet arrival time defined by its velocity and at the arrival temperature. These elements will then lose energy to the environment, previously deposited material, and the substrate. In this way we can predict the cooling rate of the deposited material and gain insight into the microstructure.

On the micro-scale, we faced a challenge in predicting the shape of a droplet upon impact. The difficulty existed because of our attempt to model a liquid with an elastic-plastic constitutive model. Such a model would be applicable after the droplet solidified. After many failed simulation attempts with ALE3D and DYNA3D to model the impact, we stepped back and tried to model a stationary liquid drop deforming under gravity (i.e., a sessile drop). We had success as shown in Figure 5. The material constants (e.g., Young's modulus) that resulted in the best fit between the analysis and experiment will be used to model the liquid. These properties will be modified for the solid phase according to a temperature dependent function found in the literature for aluminum. We plan to re-investigate the use of ALE3D and DYNA3D in predicting the deformation of a droplet on impact.

Our greatest modeling challenge is to predict the coupled thermal-mechanical response of a droplet impact. We have coupled the solid mechanics code DYNA3D with TOPAZ3D. The hardest part was developing a thermal-mechanical contact algorithm. The algorithm developed has been verified by modeling the heat transfer between two sliding blocks. Our next step is to model droplet impact. Also, other features still need to be implemented, such as, conversion of plastic work to heat.

Figure 5: The experimental sessile drop on the left helped us determine the material properties (e.g., Young's modulus) for liquid aluminum to use in our finite element model shown on the right.

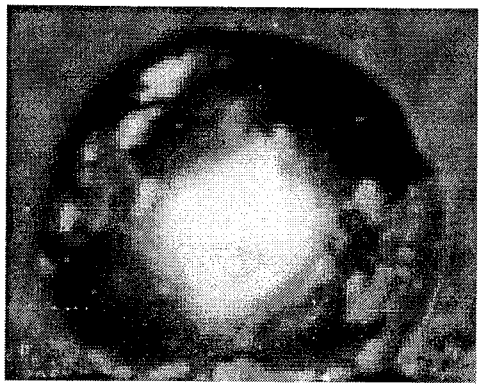

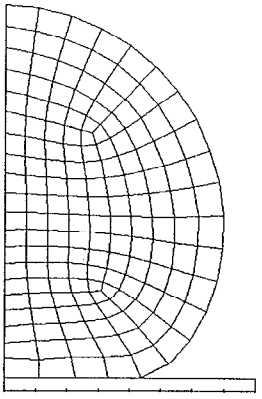

Validation, or how well the model predicts reality, is critical to our success. The literature is rich in papers investigating the splat of a liquid droplet without solidification. We found one paper describing an energy balance method that predicted the maximum splat diameter. We had good success in using this equation to predict the results in other papers. This theoretical equation was modified to include solidification and predicted a 15% greater spread diameter than measured in an experiment. We will use this equation for validation of our constitute model under development and results from the coupled DYNA-TOPAZ code effort.

Future Plans

We plan to concentrate on manufacturing simple geometric shapes (e.g. cylinders) and improve the process to decrease defects (e.g., porosity). We will use the system modeling code to determine process parameters.

HOTDROP Operation Guidelines

Wayne O. Miller
Lawrence Livermore National Laboratory
(925) 424-4472

July 20, 1999

This memo describes how to use the *HOTDROP* program for predicting the impact temperature and velocity of a liquid aluminum droplet. The program mimics the droplet casting experimental apparatus of Dr. Meilssa Orme at U. C. Irvine, Dept. of Mechanical Engineering. The program was developed as part of a collaborative LDRD between LLNL and U.C. Irvine.

Overview

HOTDROP calculates the transient temperature and position of a single molten aluminum drop as the drop falls from the orifice to the substrate. The drop may be deflected as it passes charged deflection plates. A brief report of the impact temperature and velocity of the drop is written at the end of the trajectory calculation. A full report of the transient history is also produced in a separate file.

HOTDROP input includes the major configurable parameters of the experiment. The droplet generating parameters are provided as input. They specify the initial conditions of the droplet as a function of the droplet generator. The droplet falls through a gaseous environment of either nitrogen or carbon dioxide. The gas type, pressure and temperature are specified as input parameters. The location, size and field strength of the deflection plates are specified as input, as is the droplet charge. The total vertical flight length is input. The correlations used for calculating the drag coefficient and Nusselt number are also specified as input.

HOTDROP is an extension of the *MELISSA* program. *MELISSA* was also developed at LLNL as part of the same LDRD research. Both programs are written entirely of standard FORTRAN 77, and may be run on any operating system with a FORTRAN compiler. The disk and memory requirements are minimal, and run times are typically several seconds to minutes in duration.

Input File

One input file is required for HOTRDOP, and it can have any name up to 40 characters long. The program will prompt for the input file name upon execution, and this is the only interactive input that the user provides for a run.

Appendix A of this report lists a typical input file. The header of this file describes each input parameter that is required. The input is given in four card images. The first card is an alpha-numeric title, and the remaining three cards have numerical parameter lists in free-format input.

C_D Correlations: There are three correlations that can be used for the drag coefficient. Two of them correct for close droplet spacing, and the third is for an isolated sphere. The three correlations are:

Mulholland: This correlation is based on experimental data that is valid for $90 < Re < 290$, and $1.7 < L/D < 1300$ [1].

Chiang: This correlation is based on a numerical study of three droplets moving in tandem with the free stream. It is valid for $90 < Re < 130$, and $1.3 < L/D < 6$ [2].

Isolated Sphere: This correlation is a standard form for an isolated sphere in a free stream at low Re. The coefficients are corrected by the Mulholland data for low-speed droplets (Re<290). The final form is [1]

$$C_D \text{ (isolated)} = (24/Re)(1 + 0.11\ Re^{0.687}).$$

Nu Correlations: There are three correlations that can be used for the Nusselt number. Two of them correct for close droplet spacing, and the third is for an isolated sphere. The three correlations are:

Chiang: This correlation is based on a numerical study of three droplets moving in tandem with the free stream. It is valid for $90 < Re < 130$, and $1.3 < L/D < 6$ [2].

Kleinstreuer: This correlation is based on plotted data from a numerical study by Kleinstreuer, et al. for three interacting droplets [3]. Data was available for Re = 100 and Re = 200 at L/D=6. The functional form of the correlation was developed by Salvador Aceves for the *MELISSA* program.

Isolated Sphere: This correlation is a standard form for an isolated sphere in a free stream. It is valid for $3.5 < Re < 8000$, $0.7 < Pr < 380$. The form is [4]

$$Nu = 2 + (0.4\ Re^{0.5} + 0.06\ Re^{0.67})\ Pr^{0.4}\ (\mu_\infty/\mu_s)^{0.25}$$

where μ_∞ is evaluated at the free stream temperature, and μ_s is evaluated at the surface temperature.

Correlation Locations: The deflection plates remove every other droplet, so that the L/D spacing doubles below the plates if the plates are charged. This may put the L/D ratio below the plates beyond the range of the correlations that correct for droplet spacing as noted above. The user may choose to (1) apply a corrected correlation above and below the plates, (2) apply a corrected correlation above the plates and an isolated sphere correlation below the plates, or (3) apply an isolated sphere correlation above and below the plates. The third choice is included as a reference case only and is not a good choice for droplet stream studies. These choices are available independently for the C_D and Nu correlations.

Recommended Combinations: Experience indicates that the L/D ratios expected both above and below the deflection plates are within the valid ranges for the correlations that correct for droplet spacing. Consequently it is recommended that the corrected correlations be used both

above and below the plates unless the L/D ratios begin to fall outside of the valid correlation ranges.

The choice of which corrected correlations to use is less easy to identify, and should be made to match experimental evidence. The following numerical study may help in choosing the correlation.

Correlation Study: Figure 1 gives the droplet impact temperature vs. chamber pressure results for the four recommended combinations of C_D and Nu correlations. The simulations assume initial droplet conditions of 1200 K and 10 m/s at the orifice, and use N_2 at 300 K as the fill gas. The deflection plates were not active in this study.

All of the data shown use correlations which correct for close droplet spacing both above and below the deflection plates, and this is the recommended procedure as the correlations are valid for the expected range of droplet spacing both above and below the plates. For the drag correlations, these are iCd=1 (Mulholland) and iCd=2 (Chiang), and for the Nusselt correlations, these are iNu=1 (Kleinstreuer) and iNu=2 (Chiang).

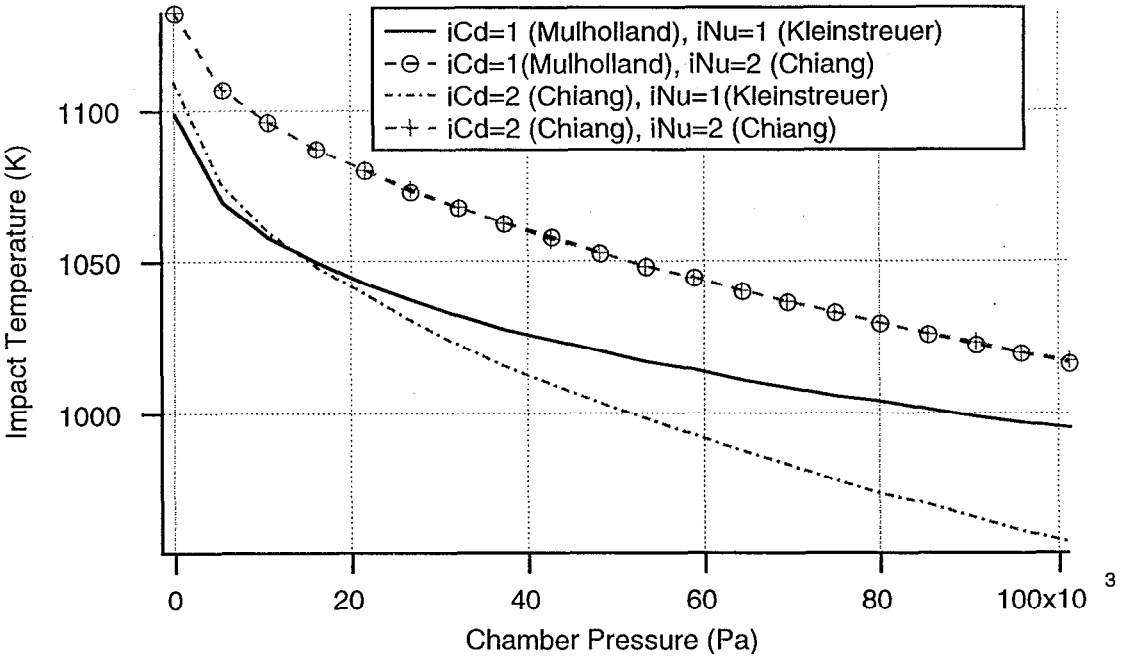

Figure 1: Impact temperature vs. chamber pressure using different full-range combinations of C_D and Nu correlations.

The main trends are as follows:

Cd: The Mulholland drag correlation predicts less drag than the Chiang drag correlation, hence faster drops. Impact velocities are relatively higher compared to the Chiang drag correlation.

Nu: The Kleinstreuer Nusselt correlation predicts higher convective heat transfer rates than the Chiang Nusselt correlation, hence faster cooling. Predicted impact temperatures are relatively cooler for Kleinstreuer than for Chiang.

Nu vs. Cd: Drag is not a function of heat transfer, hence impact velocity is not affected by the choice of Nusselt correlation. However, heat transfer is a function of velocity, so impact temperature is a function of both Nusselt and drag correlations.

It is interesting to note that the results of two correlation combinations are nearly coincident. These are the Mulholland/Chiang and Chiang/Chiang curves in Figure 1. An investigation of this did not uncover any obvious errors in the numerical solutions. It is therefore likely that the curves are members of a family of solutions that follow a commonfunctional form using a reduced set of nondimensional parameters. This possibility was not explored further.

References:

[1]. Mulholland, J. A., Srivastava, R. K. and Wendt, J. O. L., "Influence of Droplet Spacing on Drag Coefficient in Nonevaporating, Monodisperse Streams," AIAA Journal, Vol. 26, No. 10, October 1988.

[2]. Chiang, C. H. and Sirignano, W. A., "Axisymmetric Calculations of Three-Droplet Interactions," ICLASS-91 Proceedings, pp. 719-726, Gaithersburg, MD, July 1991.

[3]. Kleinstreuer, C., Wang, T-Yand Chiang, H., "Interfacial Heat and Mass transfer of Single and Multiple Drops in a Hot Gas Stream," *In* R. K. Shah (ed.), 26th National Heat Transfer Conference, ASME, Philadelphia, HTD Vol 109, ASME, New York, 1989.

[4]. Whitaker, S., "Forced Convection Heat Transfer Correlations for Flow in Pipes, past Flat Plates, Single Cylinders, Single Spheres and Flow in Packed Beds and Tube Bundles," AIChE Journal, Vol. 18, pp. 361-371, 1972.

Appendix A: HOTDROP Input File

```
*************************************************************************
*
* HOTDROP INPUT FILE
*
* Lines beginning with "*" or "$" are comment lines
*
*************************************************************************
*  v0:  initial velocity of droplet (m/s)
*  T0:  initial temperature of droplet (K)
*  xk0: dimensionless wave number for wave generator
*  r0:  droplet orifice radius (m)
*  Pgas:  fill gas pressure (Pa)
*  Tgas:  fill gas temperature (K)
*  igas:  fill gas,
*          0 = (default)
*          1 = nitrogen (default)
*          2 = carbon dioxide
*  iCD:  Drag correlation
*         0 = (default)
*         1 = Mulholland above plates, Mulholland below plates (default)
*        -1 = Mulholland above plates, isolated drop below plates
*         2 = Chiang above plates, Chiang below plates
*        -2 = Chiang above plates, isolated drop below plates
*         3 = isolated drop above and below plates
*  iNu:  Nusselt correlation
*         0 = (default)
*         1 = Kleinstreuer above plate, Kleinstreuer below plate (default)
*        -1 = Kleinstreuer above plate, Whitaker below plate
*         2 = Chiang above plate, Chiang below plate
*        -2 = Chiang above plate, Whitaker below plate
*         3 = Whitaker above and below plate
*  yflight:  total vertical trajectory distance (m)
*  yplate1:  distance from orifice to top of deflection plate (m)
*  yplate2:  distance from orifice to bottom of deflection plate (m)
*  Vc:  charge electrode voltage (V)
*  Ed:  deflection plate electric field (V/m)
*************************************************************************
*
*** title card
*
Here's a title for this run
*
*** control card 1: v0, T0, xk0, r0
*
*10. 1200. 0.697 50.e-6
10. 1200. 0.697 50.e-6
*
*** control card 2: Pgas, Tgas, igas, iCd, iNu
*
*101325. 300. 1 1 1
101325. 300. 1 -1 2
*
*** control card 3: yflight, yplate1, yplate2, Vc, Ed
*
*0.500 0.177 0.217 400. 6.e5
0.500 0.177 0.217 0. 0.
```

Appendix B: HOTDROP Summary File

*** p r o b l e m t i t l e ***

Here's a title for this run

*** c o n t r o l d a t a ***

control card 1

droplet initial velocity (m/s)	=	10.00
droplet initial temperature (K)	=	1200.
droplet generator wave number	=	0.6970
orifice radius (m)	=	0.5000E-04

control card 2

chamber gas pressure (Pa)	=	0.1013E+06
chamber gas temperature (K)	=	300.0
chamber gas	=	1

eq.0: (set to default value)
eq.1: nitrogen (default value)
eq.2: carbon dioxide

drag correlation = -1

eq.0: (set to default value)
eq.-2: Chiang above plate
isolated sphere below plate
eq.-1: Mulholland above plate
isolated sphere below plate
eq.1: Mulholland above plate
Mulholland below plate (default value)
eq.2: Chiang above plate
Chiang below plate
eq.3: isolated sphere above plate
isolated sphere below plate

Nusselt correlation = 2

eq.0: (set to default value)
eq.-2: Chiang above plate
isolated sphere below plate
eq.-1: Kleinstreuer above plate
isolated sphere below plate
eq.1: Kleinstreuer above plate
Kleinstreuer below plate (default value)
eq.2: Chiang above plate
Chiang below plate
eq.3: isolated sphere above plate
isolated sphere below plate

control card 3

total flight distance (m)	=	0.5000
orifice to top of deflection plate (m)	=	0.1770
orifice to bottom of deflection plate (m)	=	0.2170
charge electrode voltage (V)	=	0.
deflection plate electric field (V/m)	=	0.

*** s o l u t i o n d a t a ***

droplet generator data

generation frequency (1/s)	=	0.2219E+05
droplet radius (m)	=	0.9455E-04
droplet volume (m^3)	=	0.3541E-11
droplet mass (kg)	=	0.8385E-08
generator mass flow rate (kg/s)	=	0.1860E-03
generator volume flow rate (m^3/s)	=	0.7856E-07

initial droplet state

time (s)	=	0.
droplet vertical velocity (m/s)	=	10.00
droplet horizontal velocity (m/s)	=	0.
droplet temperature (K)	=	1200.
droplet spacing ratio (L/D)	=	2.383

final (impact) droplet state

time (s)	=	0.5217E-01
vertical trajectory distance (m)	=	0.5000
horizontal trajectory distance (m)	=	0.
droplet vertical velocity (m/s)	=	8.975
droplet horizontal velocity (m/s)	=	0.

```
droplet temperature (K)                    =   1133.

droplet spacing ratio (L/D)                =   2.139

Re (metal properties)                      =   3092.

We (metal properties)                      =   39.47

T_droplet - T_melt (K)                     =   199.3

droplets did not coalesce
```

APPENDIX C: HOTDROP HISTORY FILE (Abbreviated)

time	x	y	vel	temp	Cd	Re	L/D	h		
1.0000E-04	0.0000E+00	9.9995E-04	9.9990E+00	1.1999E+03	1.0468E+04	1.2193E-03	2.3832E+00	1.3297E+02		
2.0000E-04	0.0000E+00	1.9998E-03	9.9979E+00	1.1997E+03	1.0468E+04	1.2192E-03	2.3830E+00	1.3296E+02		
3.0000E-04	0.0000E+00	2.9995E-03	9.9969E+00	1.1996E+03	1.0469E+04	1.2191E-03	2.3827E+00	1.3296E+02		
.										
.										
.										
6.1156E-02	0.0000E+00	4.9891E-01	5.8425E+00	1.0210E+03	1.0241E+00	7.2189E+01	1.3925E+00	2.0453E+02		
6.1256E-02	0.0000E+00	4.9950E-01	5.8366E+00	1.0208E+03	1.0247E+00	7.2117E+01	1.3911E+00	2.0418E+02		
6.1343E-02	0.0000E+00	5.0000E-01	5.8316E+00	1.0207E+03	1.0252E+00	7.2054E+01	1.3899E+00	2.0387E+02		

Spray Deposition Modeling with ALE3D

Comparison of Results with Madjeski's Model Assuming No Freezing of the Droplet

Final Status Report

January 29, 1999

Vivek Sahai

Lawrence Livermore National Laboratory
University of California
P.O. Box 808, L-140
Livermore, CA 94551

Development of methods to spray form materials which use methods of precisely controlled deposition of droplets can result in new manufacturing processes which offer improved metallurgical performance and reduced costs. Segregation can be controlled due to the rapid solidification of the droplets which gives a fine microstructure to the part. Freeform fabrication allows for savings in both material usage as well as energy usage. The key to developing the process is control of the droplet and understanding how the droplets interact with each other and the substrate. This report documents the procedure of how a three dimensional lagrange-eulerian code was used to simulate the impact of a droplet against a substrate.

To understand the droplet-substrate impact, simulations were run using an Arbitrary Lagrange-Eulerian Code (ALE3D[1]). ALE3D was run to simulate the deformation of pure aluminum spherical droplets on an aluminum substate. These simulations neglected the heat transfer effects at the droplet/substrate interface. The maximum predicted splat diameter (Dmax/ Do) was then compared to predictions from Madjeski's model[2]. The cases studied are given below in Table 1. These cases are in the range of operating conditions expected for the experimental apparatus used by Orme[3] at UC-Irvine. The low values of the Weber Number indicate the importance of capillary effects. Pasandideh-Fard[4] showed that under conditions of no freezing that capillary effects can be neglected if the Weber

Number is much greater than the square root of the Reynolds number. This is clearly not the case for the situations given in Table 1.

Table 1. Dimensions of Aluminum Droplet and Speed Before Impact Examined With Madjeski's Model and ALE3D

Diameter of Droplet	Speed of Droplet	Reynolds Number	Weber Number
200μm	5 m/s	1834.6	13.04
200μm	10 m/s	3669.2	52.19
100μm	5 m/s	917	6.5235
100μm	10 m/s	1834.6	26.094

The material model used in the ALE3D calculations (known as material model number 58 in ALE3D) was formulated to examine melting and solidification effects. Unfortunately, this model can only work for brick element type meshes. This model has been used in the simulation of melting and solidification of aluminum alloys and for solid deformation modeling of metal forming processes. The constants given on the ALE3D website for this model are for an Aluminum alloy(2021). The equation of state used in the model are briefly described below (see ALE3D users manual[1] or the website at the location http://www.llnl.gov/llnl_only/bdiv/ale3d/ for more explanation):

$$p = B\mu + \gamma Em$$

where B is bulk modulus, μ is the reciprocal of the compression minus one, γ is equal to $B\alpha/\rho Cp$, α is the thermal diffusivity, ρ is the density, Cp is the specific heat, and Em is the material energy. The bulk modulus can vary from a complete solid to liquid as given by:

$$B=FS(T)Bsol + (1-FS(T))Bliq$$

where FS(T) is the fraction solid variation as function temperature (T), Bliq is the liquid bulk modulus, and Bsol is the solid bulk modulus given by $Bsol = E/(3(1-2Yp)$ where E is the elastic modulus which can be temperature dependent ($E= Eo - E_1T$), and Yp is Poisson's ratio.

Along with the above equation of state, a constitutive equation is solved to determine the flow stress, σ :

$$\varepsilon_s = A(\sinh(\beta\sigma))^n \exp(-\Delta H/RT)$$

where ε_s is the strain, R is the gas constant, ΔH is the activation energy, and the quantities A, β, and n are material constants. Once the flow stress is determined it is modified by multiplying it by the fraction solid of the material to determine the effective flow stress. A final feature of the model is the ability to specify a coherency temperature, a temperature above which all the stresses are set equal to zero. The model was run by adding viscous effects. It should be noted that the model does not consider the effects of surface tension of the droplet which is very important based on the values of the Weber number given in Table 1. Although viscosity as a function of temperature can be input into the model, only a constant viscosity was used since most of the analyses dealt with isothermal conditions. Some of the aluminum material properties used in the ALE3D simulations are given in Table 2. This material model is used with properties of the drop in the fluid state (i.e. with an assigned viscosity and initial temperature above the liquidus) with no freezing considered across the droplet-substrate interface.

Table 2. Aluminum Material Properties Used in the ALE3D Calculations

Density:	2368 kg/m^3
Viscosity:	1.275E-3 kg/m sec
Activation Energy, ΔH :	1.344e5 J
Elastic Modulus E_o :	69E+9 N/m^2
Liquid Bulk Modulus, B_{liq}:	4.8E+10 N/m^2
Material Constants A, β, n :	3.45E+8, .025E-6, 3.8

These results were then compared to a refined form of Madjeski's model which is a differential equation of the droplet formation as a function of a freezing parameter, Reynolds number and Weber number. A comparison has been performed with Madjeski's results with those experiments and other fluid mechanics and heat transfer models reported in the literature. Madjeski calculates droplet shape assuming the droplet transforms into a cylinder taking into account energy loss due to the transformation. The modified form of Madjeski's model used for the initial spreading of the droplet is given below:

$$\left[\frac{dR}{dt}\right]_{t=0} = w\sqrt{\frac{\frac{5e}{3}+\frac{20}{We}\left(e-\varepsilon^2-\frac{1}{3e}\right)}{1+\frac{11}{252\varepsilon^6}}}$$

Here, dR/dt is the change in radius of the cylinder at the beginning of impact, w is the initial droplet velocity before impact, e is the ratio of cylinder energy after impact to the droplet energy before impact (e = 0.6 in this study for the cases of We >7.7, indicating a loss of energy of 40%, and e=0.9 in this study for the case with We = 6.5, indicating a loss of energy of 10%), ε is the ratio of initial radius of the cylinder to initial droplet diameter, and We is the Weber number. The results obtained by Aceves et.al.[5] of this equation has shown that this model predicts the final splat diameter within 30 percent of the reported values. This model was solved for the cases listed in Table 1.

The ALE3D model was set and run in the following manner. First, a mesh was created by Truegrid[6] which took advantage of the symmetry of the drop by using symmetry planes to mesh only 90 degrees of the drop. The mesh dimensions were chosen based on the results from Madjeski's method. The height of the mesh above the droplet/substrate interface was 0.25 mm, and length and width of the mesh was 0.5 mm. The mesh was graded in the direction perpendicular to the droplet/substrate interface. The cases listed in Table 1 were run with a mesh in which the total number of nodes was 8959. This mesh represented a tradeoff between acceptable running time and resolution of the droplet dynamics of impacting the substrate and spreading. On the planes of symmetry, appropriate displacement boundary conditions were specified in Truegrid. Once the mesh was created, a file was created for GEN3D[1]. This gives the material parameters needed by the ALE3D model described above along with various run parameters, the initial radius of the droplet, it's position above the droplet/substrate interface (0.11 mm), and its velocity before impact. The droplet is actually superimposed on the mesh using the shape command in the GEN3D input file. This file along with the Truegrid mesh is used to produce the input file for ALE3D. The case was then run in ALE3D saving results every 0.5 micro seconds to view in the postprocessor, MESHTV[7]. The droplet diameters could be estimated upto +/- 5 microns from viewing the MESHTV results. ALE3D determines the motion of the droplet through the mesh, showing droplet impact and spreading along the substrate. These cases were run on the lab's compass cluster machines with maximum run times of 72 hours. Some attempts were made by decreasing the run time by varying

parameters such as the increasing the advection cycling parameter without much success. From the viewing of the results, the changes of droplet shape could be noted. The maximum splat diameters were then estimated from these results and compared to Madjeski's model as described above.

Before, obtaining results with ALE3D a few studies were performed. The first study was to understand the sensitivity of the results of droplet spreading by analyzing different types of conditions at the droplet/substrate interface on droplet spreading. The second study was to determine the size of mesh in order to obtain mesh insensitive results in ALE3D. Finally after these studies were completed, results for the four cases listed in Table 1 using ALE3D were obtained.

First, different types of conditions at the droplet/substrate interface were examined. There are four types of conditions that can be used in ALE3D at this interface. They are: fixing the displacements at the droplet/substrate interface to act as a no slip condition for the droplet at this interface; using a tied slide surface; setting a friction force along the slide surface; and specifying a slide surface with voids at this interface. The results showed that there was no difference in predictions in maximum droplet diameter by either specifying that the displacements are fixed at the droplet/substrate interface or by tying the slide surface to the fixed substrate. When only friction was specified or sliding with voids was chosen, then there was no slowing of the droplet, i.e. the motion of the droplet continued indefinitely, hitting the symmetry planes and bouncing back. Increasing the magnitude of the friction force as much as 25 times the original value did not result in any changes in this behavior. It was decided then to use the tied slide surface methodology in all future runs of ALE3D. It was also interesting to note that for the 200 micron, 10 m/s droplet case that changes of 25% on bulk liquidus, and the activation energy resulted only in differences of less than 1% in the predicted maximum droplet diameter.

Finally, different size meshes were analyzed in ALE3D for the 200 micron, 10 meter per second droplet case. Mesh sizes of 2800 nodes, 6300 nodes, 8959 nodes, and 16,758 nodes was studied. Based on the time varying splat diameter prediction from ALE3D, it was determined that the 8959 node mesh gave results within 3% of the 16,758 nodes mesh. This was the mesh used to run the cases given above in Table 1.

The results of ALE3D as compared to Madjeski's model without considering freezing effects are given below in Table 3. The predictions in maximum splat diameter from

ALE3D agree within 30 % of the values predicted by Madjeski. It is interesting to note from the results that when the Weber number is low, the error in maximum splat diameter increases. Figure 3 shows the ALE3D predictions for the change in droplet diameter vs. time against the Madjeski predictions. The ALE3D results show that the time to reach the maximum splat diameter is greater than predicted by Madjeski.

Table 3. Comparison of ALE3D Results with Madjeski's Model

Droplet Diameter	Droplet Speed	Dmax/Do ALE3D	Dmax/Do Madjeski	%Error
200μm	5 m/s	3.4	2.66	28%
200μm	10 m/s	4.6	4.2	10%
100μm	5 m/s	2.68	2.19	22%
100μm	10 m/s	2.92	3.28	11%

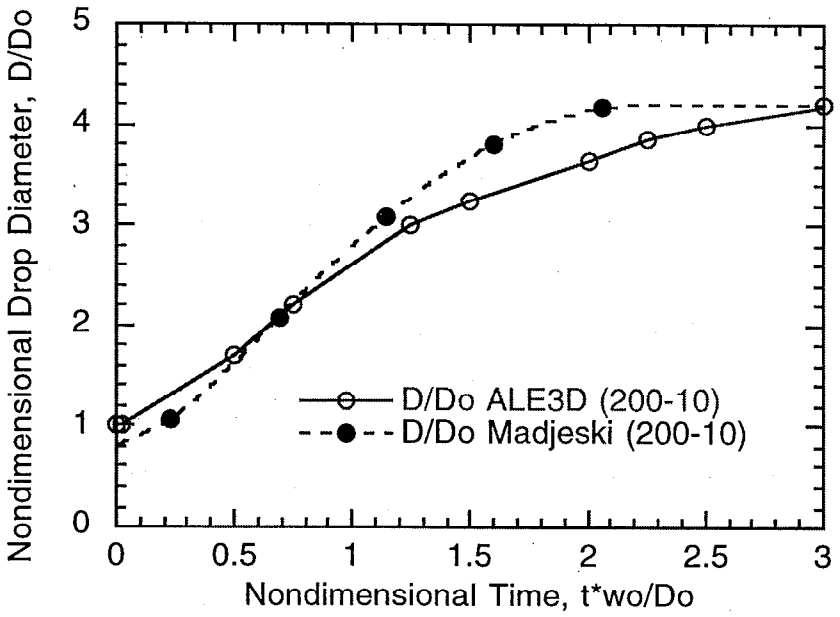

Figure 1. Comparison of change of droplet diameter with respect to nondimensional time (time*velocity/initial diameter) for 200 micron diameter droplet with a velocity before impact of 10 m/s with Madjeski's model[5] results.

A few cases were run with the ALE3D model considering non-isothermal effects. In these simulations, the default values of the material model were used. An initial temperature of the droplet needs to be estimated. For a drop falling in a vacuum, the convection from the drop can be neglected and using a lumped capacitance analysis(valid when the Biot number is less than 0.1) the equation governing the loss of heat from the drop via radiation can be expressed as:

$$\rho V C_p \, dT/dt = -\varepsilon_m \sigma_{sb} A(T^4 - T_{sur}^4)$$

where ρ is the density of the drop, V is the volume of the drop, Cp is the specific heat of the drop, ε_m is the emissivity of the drop, σ_{sb} is the Stefan-Boltzman constant, A is the surface area of the drop, and Tsur is the temperature of the surroundings. Assuming Tsur = 0, then this equation yields a solution of (by integration from t=0 to t):

$$t = \rho V c/(3\varepsilon_m A\sigma_{sb}) (1/T^3 - 1/Ti^3)$$

where Ti is the initial temperature of the drop. Knowing the distance and speed before impact, then the above equation was used to estimate the initial temperature of the droplet before impact. If the droplet is falling through a gas, then forced convection effects are very important and must be included in the analysis. Orme[3] has shown that significant undercooling can occur in the droplet temperature as the drop approaches the substrate.

Using ALE3D, a few cases were attempted with non-isothermal effects(i.e. freezing of the drop). The gas surrounding the drop was changed to a void material. The radius of the drop examined was 50 microns and its speed before impact was 5 m/s. There were many difficulties encountered in trying to obtain a solution to the problem. The initial temperature of the void material had to be set to the initial temperature of the drop in order to get a solution. Otherwise, the time step would be severely diminished to excessive subcycling. Before the droplet impacted the plate, there was evidence of heat transfer from the void to the plate. This unneeded effect was diminished somewhat by lowering the thermal conductivity of the void material. For temperatures of the droplet above the liquidus, no solution could be obtained. For initial temperatures below the liquidus temperature (in the mushy zone) a few solutions could be obtained. The run times were quite long for the 10,400 node meshes (52 hours) for a solution out to 22 microseconds. A couple of runs showed the importance of contact conductance at the droplet/substrate interface. At a contact conductance of $1X10^5$ W/m^{2}K there is substantial spreading of the drop. However at a contact conductance of $1X10^6$ W/m^{2}K, there was not much movement of the drop at all since the heat transfer from the drop to the substrate is substantially increased cooling the

droplet to below its coherency temperature and restricting the spreading of the drop along the substrate. The importance of knowing the value of the heat transfer coefficient at the droplet/substrate agrees with the observations made by Liu[8] and Pasandideh-Fard[4]. However, the inability to resolve the convergence problems led to abandoning of the effort to explore droplet freezing.

The analyses using ALE3D to understand droplet/substrate interaction led to the following conclusions and recommendations for future work:

1) Mesh effects are important part of coming up with a good solution technique. The solutions must be checked for mesh sensitivity.

2) It was determined that either using a tied slide surface or a fixed displacement boundary condition in ALE3D gave reasonable drop spreading characteristics. It is noted that sliding with voids or using friction effects at the droplet/substrate interface produced an infinite type of droplet spreading.

3) Despite the long run times and convergence problems, ALE3D can be used as a tool to help predict the final droplet splat diameter.

4) The predictions are within reason when compared to the semi-analytic solution of Madjeski. It was interesting to note that the maximum errors between ALE3D and Madjeski occur when the Weber number is low.

5) More improvement is needed in developing a robust solver in ALE3D to solve the conjugate problem.

6) The few solutions obtained including freezing effects of the drop show the importance of knowing the heat transfer coefficient at the droplet/substrate interface. It is important during the experimental runs to track the temperatures in the plate at various depths/locations on which the droplet falls. This information could be used in an inverse analysis[9] to determine the heat flux at the droplet/substrate interface. The use of an infrared camera or pyrometer is suggested to obtain information on droplet temperatures.

6) ALE3D needs to include the effects of surface tension in the analysis. A possible way to include surface tension effects is to run a ALE3D case of a liquid drop sitting on the

substrate and modify the material model parameters until the shape conforms to the correct as predicted from the balance of the forces due to surface tension. This measurement of equilibrium shape due to gravity alone of sessile drops for has been used as a measuring technique for surface tension(see, Butler and Bloom[10]). However, to do these types of analyses, MESHTV will need to be able to print out the coordinates of the droplet interface. This is a capability that does not exist right now.

7) To increase run time by decreasing the size of the mesh, a 2-D axi-symmetric version of the problem needs to be attempted.

8) Because of the long run times involved, other fluid dynamic codes such as Telluride and/or FLOW3D need to be examined as alternatives to solve these types of problems. Both of these codes have capabilities to look at aspects of these types of problems. These codes overcome the shortcommings of using the structural/mechanical codes and ALE3D by including surface tension effects which are very important. In fact, FLOW3D was used in an isothermal analysis by Trapaga[11] of the impact of lead droplets on a substrate. ALE3D was set up to analyze one of these cases but due to the need for devloping large meshes which have long run times, the analysis was not completed.

References

[1] Steve Anderson, Evi Dube, Scott Futral, Al Nichols, Ivan Otero, Richard Sharp, "Users Manual for ALE3D", Draft Version, Internal Lab Document, April 21, 1998.

[2] J. Madjeski, "Solidification of Droplets on a Cold Surface", International Journal of Heat and Mass Transfer, Volume 19, pp. 1009-1013, 1976.

[3] Melissa E. Orme, Changsheng Huang, and Jon Courter, "Precision Droplet-Based Manufacturing and Material Synthesis: Fluid Dynamics and Thermal Control Issues", Atomization and Sprays, Vol. 6, pp.305-329, 1996.

[4] M. Pasandideh-Fard, R. Bhola, S. Chandra, J. Mostaghimi, "Deposition of Tin Droplets on a Steel Plate: Simulations and Experiments", International Journal of Heat and Mass Transfer, Volume 41, pp. 2929-2945, 1998.

[5] Salvador M. Aceves, Vivek Sahai, and Art Shapiro, "An Accuracy Evaluation for the Madjeski Splat-Quench Solidification Model", Lawrence Livermore National Laboratory Report to be submitted to ASME International Congress meeting, Fall 1999.

[6] Truegrid, A Mesh Generation Tool from XYZ Corporation, Livermore, CA.

[7]MeshTV Command Line Interface Manual, UCRL-MA-127443, June 29, 1998, Version 3.1.

[8] W. Liu, G.X. Wang, and E.F. Matthys, "Thermal Analysis and Measurements for a Molten Metal Drop Impacting on a Substrate: Cooling, Solidification, and Heat Transfer Coefficient", International Journal of Heat and Mass Transfer, Vol. 38, pp. 1387-1395, 1995.

[9] Vivek Sahai, Salvador Aceves, and Werner Stein, "Explanation of How to Run the Global Local Optimization Code (GLO) to Find Surface Heat Flux, Lawrence Livermore National Laboratory Report, 1998.

[10] James N. Butler, and Burton H. Bloom, "A Curve-Fitting Method For Calculation Interfacial Tension From the Shape of a Sessile Drop", Surface Science, pp. 1-17. 1966.

[11] Gerardo Trapaga, and Julian Szekely, "Mathematical Modeling of the Isothermal Impingement of Liquid Droplets in Spraying Processes", Metallurgical Transactions B, Volume 22B, pp. 901-914, December 1991.

Proceedings of IMECE'99
1999 ASME International Mechanical Engineering Congress and Exposition
November 14-19, 1999, Nashville, Tennesee, USA

ESTIMATING THE MAXIMUM SPLAT DIAMETER OF A SOLIDIFYING DROPLET

Nicolas G. Hadjiconstantinou
Lawrence Livermore National Laboratory
L-228
Livermore, California 94551
Email: hadjiconstantinou1@llnl.gov

ABSTRACT

We present a simple analytical model for the estimation of the maximum splat diameter of an impacting droplet on a subcooled target. This work is an extension of the isothermal model of Pasandideh-Fard et al. (1996). The model uses an energy conservation argument, applied between the initial and final drop configurations, to approximately capture the dynamics of spreading. The effects of viscous dissipation, surface tension, and contact angle are taken into account. Tests against limited experimental data at high Reynolds and Weber numbers indicate that an accuracy of the order of 5% is achieved with no adjustable parameters required. Agreement with experimental data in the limit $We \to \infty$ is also very good. We additionally propose a simple model for the estimation of the thickness of the freezing layer developed at the droplet-substrate contact during droplet spreading. This model accounts for the effect of thermal contact resistance and its predictions compare favorably with experimental data.

NOMENCLATURE

c_p Specific heat per unit mass.
D_0 Initial droplet diameter.
D_m Final disk diameter.
h Final disk thickness.
h_c Contact resistance heat transfer coefficient.
h_f Stagnation point flow heat transfer coefficient.
h_{fg} Latent heat per unit mass.
h_s Solidified layer heat transfer coefficient.
h_t Total heat transfer coefficient.
k Liquid metal thermal conductivity.
k_s Solid metal thermal conductivity.
KE_1 Initial drop kinetic energy.
Nu_c Contact resistance Nusselt number.
Nu_f Stagnation point flow Nusselt number.
Nu_s Solidified layer Nusselt number.
Nu_t Total Nusselt number.
r Radial coordinate.
Re Reynolds number.
s Solidified layer thickness.
$\bar{s}$ Time averaged solidified layer thickness.
s^* Non-dimensional solidified layer thickness ($= s/D_0$).
SE_1 Initial drop surface energy.
SE_2 Final disk surface energy.
Ste Stefan number ($c_p(T_m - T_w)/h_{fg}$).
Ste_T Stefan number based on temperature T ($= c_p(T - T_w)/h_{fg}$).
T Solidified layer final (average) temperature.
T_0 Droplet initial temperature.
T_m Droplet melting temperature.
T_w Substrate temperature.
u Radial velocity.
V Excluded volume.
V_0 Initial droplet velocity.
W Work done on deforming droplet.
We Weber number.

Greek symbols
β $= \rho/\rho_s$
γ Surface tension.
δ Boundary layer thickness.
θ_a Advancing contact angle.
μ Viscosity.
ξ Spread ratio ($= D_m/D_0$).

ρ Liquid density.
ρ_s Solid density.
τ Estimated droplet arrest time.
ω Flow parameter.

INTRODUCTION

In recent years various simple analytical models for the estimation of the maximum splat diameter of an impacting droplet on a subcooled target have been proposed. Such models could prove very useful as preliminary design tools in the rapidly developing field of microfabrication. They can additionally facilitate the understanding of the coupled droplet spreading and solidification dynamics, which will lead to improvements in microfabrication quality. In this paper we present a model that accounts for the effects of surface tension, contact angle, and solidification at the droplet-target interface.

Consider a superheated liquid metal droplet of diameter D_0 and at temperature $T_0 > T_m$, impacting a subcooled solid substrate (temperature $T_w < T_m$) with velocity V_0. We are interested in the limit of small superheat, that is $T_0 - T_m \to 0$ where T_m is the melting temperature. When spreading stops, the droplet has reached the maximum splat configuration in the shape of a thin disk of diameter D_m and height h. We assume that the material has partially solidified: a thin layer of thickness s (averaged over the diameter) at the substrate-droplet interface is now solid at (an average) temperature T, where $T_w < T < T_0$, and the remaining droplet material is molten at T_m. The maximum splat ratio ξ is defined as $\xi = D_m/D_0$. One important assumption used in this work is that the droplet arrest is not governed by solidification, that is the effect of heat transfer and solidification is only secondary to the spread process. This assumption is somewhat limiting, but its wide use in the literature (Madejski, 1976; Bennett and Poulikakos, 1994; Pasandideh-Fard et al., 1998) has shown that is very reasonable for a wide range of controlling parameters. A recent critical review by Bennett and Poulikakos (1994) emphasizes the inadequacy of the Stefan problem approach to capture the freezing kinetics and their effect on the droplet spreading and arrest. Further evidence to this effect is given in the work of Pasandideh-Fard et al. (1998): in addition to showing the Stefan problem approach to be very inaccurate, it also suggests that the thermal contact resistance between the target and the droplet plays an important role in the freezing layer growth. The importance of the substrate properties was also reported in the work of Collings et. al (1989).

The model presented in this paper is an extension of the isothermal model for the maximum spread diameter by Pasandideh-Fard et al. (1996). In the isothermal case the target and droplet are at the same temperature ($T_0 = T_w$) and negligible heat exchange takes place between the two. The isothermal model was extended to the non-isothermal case by the above authors in (Pasandideh-Fard et al., 1998). Although agreement with experimental data was demonstrated, the validity of some of the approximations in that model is questionable. The present paper suggests a more appropriate formulation which also improves agreement with experimental data. We additionally propose a model for the estimation of the thickness of the thin frozen layer at the droplet-target interface that is important for the calculation of the maximum splat diameter.

THE MAXIMUM SPLAT DIAMETER

Isothermal model

We briefly describe the isothermal model presented by Pasandideh-Fard et al. (1996) for completeness. The maximum spread diameter, D_m, can be estimated by using an energy conservation argument: the energy at every instant in time, and hence at the maximum splat diameter configuration (configuration 2), has to equal the initial energy of the drop (configuration 1). This initial energy is equal to the sum of the kinetic energy (KE_1) and the surface energy (SE_1) of the impacting droplet. The kinetic energy is given by:

$$KE_1 = \left(\frac{1}{2}\rho V_0^2\right)\left(\frac{1}{6}\pi D_0^3\right), \tag{1}$$

where ρ is the liquid drop density. The initial surface energy is given by:

$$SE_1 = \pi D_0^2 \gamma, \tag{2}$$

where γ is the surface tension coefficient for the drop in the ambient environment.

The energy at the maximum splat configuration consists of the energy dissipated through the action of viscosity during the spreading process and the surface energy of the maximum splat configuration. The first term has been shown (Pasandideh-Fard et al., 1996) to (approximately) equal

$$W = \frac{\pi}{3}\rho V_0^2 D_0 D_m^2 \frac{1}{\sqrt{Re}} \tag{3}$$

where $Re = \rho V_0 D_0/\mu$ is the Reynolds number. This estimate is obtained by assuming an axisymmetric stagnation point flow which in the high Reynolds limit can be

approximated by a viscous boundary layer of thickness $\delta = 2D_0/\sqrt{Re}$, and potential flow outside this boundary layer.

The surface energy (SE_2) is estimated by assuming that the final configuration approximates a thin disk. It is shown by Collings et al. (1989) that given the contact angle (θ_a), and the disk-shape geometry assumption with diameter D_m and height h that is small compared to D_m,

$$SE_2 = \frac{\pi}{4} D_m^2 \gamma (1 - \cos\theta_a). \tag{4}$$

Equating

$$KE_1 + SE_1 = W + SE_2, \tag{5}$$

yields an expression for the spread ratio $\xi = D_m/D_0$ which has been shown to reproduce experimental results satisfactorily (Pasandideh-Fard et al., 1996).

It is important to note that the stagnation flow model used for the calculation of the viscous effects predicts that the droplet spreading stops after time τ, where

$$\tau = \frac{8D_0}{3V_0}. \tag{6}$$

This is important since in the non-isothermal case considered below we assume that spreading is inhibited by viscous and surface tension effects and hence, spreading stops at the same time as the isothermal case.

Non-isothermal spreading

In the non-isothermal case, the effects of solidification have been accounted for in the work of Pasandideh-Fard et al. (1998) by including in the above energy balance a fictitious "lost kinetic energy" term. The kinetic energy of configuration 2, however, is already assumed to be zero in the above energy balance. We believe that, although this term results in a spread factor that is in reasonable agreement with experimental data, it does not adequately represent the physics of solidification. The solidification process manifests itself through the latent heat which should enter the energy balance; if thermal effects cannot be included in the model because of the insufficient understanding of their relative importance, the whole of the solidified material can be excluded. We propose a modification to the above energy balance that correctly captures the effect of phase change and results in a similar expression for the spread factor which is, however, not ad-hoc. In what follows we show that the ad-hoc "lost kinetic energy" term can be motivated as part of the solidified material energy which is not included in our modified energy balance.

The effect of phase change is accounted for by applying the energy balance to the liquid that does not solidify. Following Pasandideh-Fard et al. (1998), we estimate the solidified mass as $\pi\rho_s D_m^2 s$. This material is then excluded from the energy balance $KE_1 + SE_1 = W + SE_2$ under the assumption that negligible thermal energy exchange takes place between the solidified and unsolidified parts of the drop. We believe that this assumption is not unreasonable; the high Reynolds number stagnation flow model inside the drop, which gives reasonable results for the viscous heat generation, involves little mixing and mostly entrainment of the fluid from the potential flow region towards the wall ($RePr \sim 100 \gg 1$). The new terms in the energy balance are now:

$$KE_1 = \left(\frac{1}{2}\rho {V_0}^2\right)\left(\frac{1}{6}\pi {D_0}^3 - \frac{\pi}{4}\frac{\rho_s}{\rho} D_m^2 s\right), \tag{7}$$

and

$$W = \frac{\frac{\pi}{6}\rho {D_0}^3 - \frac{\pi}{4}\rho_s D_m^2 s}{\frac{\pi}{6}\rho D_0^3}\frac{\pi}{3}\rho {V_0}^2 D_0 D_m^2 \frac{1}{\sqrt{Re}}, \tag{8}$$

which lead to a new expression for ξ:

$$\xi^2 = \frac{\omega(Re, We, \theta_a, s^*)}{12\frac{We}{\sqrt{Re}}\beta s^*} - \frac{\sqrt{\omega^2(Re, We, \theta_a, s^*) - 24\frac{We}{\sqrt{Re}}\beta s^*(We + 12)}}{12\frac{We}{\sqrt{Re}}\beta s^*}, \tag{9}$$

where

$$\omega(Re, We, \theta_a, s^*) = \frac{4We}{\sqrt{Re}} + 3(1 - \cos\theta_a) + \frac{3}{2}\beta s^* We, \tag{10}$$

$\beta = \rho_s/\rho$, and $s^* = s/D_0$.

Note that the surface terms SE_1, and SE_2 were not corrected for the reduced mass. In the case of SE_1, the correction is of smaller order because surface effects scale as $V^{2/3}$, where V is the excluded volume ($= \pi D_m^2 s/4$). Neglecting this correction should be reasonable in the high Weber number limit for which this model is intended. In the case of SE_2, the existence of a solid layer between the molten material and the substrate will not affect expression (4) if the interfacial energy between the substrate and

the liquid is not significantly different than the interfacial energy between the liquid and the solid metal.

Taking $\beta \approx 1$, we obtain the following results for the three experimental cases (varying subcooled target temperature T_w) presented by Pasandideh-Fard et al. (1998). For $T_w = 240^oC$, $s^* = 0$, $\xi = 3.24$ and the experimental value is $\xi = 3.3$; for $T_w = 150^oC$, $s^* = 0.014$, $\xi = 3.06$, and the experimental value is $\xi = 3.1$; for $T_w = 25^oC$, $s^* = 0.035$, $\xi = 2.8$, and the experimental value is $\xi = 2.9$. The values of s^* used were obtained from the numerical simulations of Pasandideh-Fard et al. A model for the estimation of s^* is given in the next section.

We see that the our model improves the accuracy of the previous model while being based on a more theoretically sound framework. We can now see the physical significance of the "lost kinetic energy" term in Pasandideh-Fard et al. (1998); it results from the exclusion of the solidified portion of the drop (equation (7)) from the energy balance (equation (5)). One assumption used in the above derivation is that the heat generated from the viscous dissipation is uniformly distributed in the drop volume, and hence it is proportionally distributed to the solidified and unsolidified parts of the droplet (equation (7)). The agreement with the experimental data above suggests that this assumption is reasonable, or that its effect is small.

We can alternatively assume that mixing in the droplet is minimal, and hence the heat generated by viscous dissipation is "retained" within the viscous boundary layer thickness. In this minimal mixing case, the ratio of the thickness between the solidified layer and the viscous dissipation boundary layer (δ) is important. The equivalent of equation (7) is now:

$$W = \left(\frac{\frac{\delta}{D_o}}{\frac{\delta}{D_o} + s^*} \right) \frac{\pi}{3} \rho {V_o}^2 D_o D_{max}^2 \frac{1}{\sqrt{Re}}. \qquad (11)$$

When s^* is large, the material close to the wall, which is within the viscous boundary layer, solidifies and $W \to 0$. Conversely, if $s^* \to 0$, then all of the viscous energy generation is included in the part of the droplet that does not solidify. This modified term results in a new expression for ξ:

$$\xi = \sqrt{\frac{We + 12}{\frac{3}{2}\beta We s^* + 3(1 - cos\theta_a) + 4\frac{We}{\sqrt{Re}}\left(\frac{2}{2+s^*\sqrt{Re}}\right)}}. \qquad (12)$$

This expression gives the following results for the experimental data presented above: for $T_w = 240^oC$, $s^* = 0$, $\xi = 3.24$ and the experimental value is $\xi = 3.3$; for $T_w = 150^oC$, $s^* = 0.014$, $\xi = 3.17$, and the experimental value is $\xi = 3.1$; for $T_w = 25^oC$, $s^* = 0.035$, $\xi = 2.89$, and the experimental value is $\xi = 2.9$. This alternative expression seems to give results comparable in accuracy to the previous one (equation (9)). It seems that equation (9) tends to underestimate the value of ξ, and equation (12) tends to overestimate the value of ξ. The exact physics must be some compromise between the two assumptions leading to equations (9) and (12). Additional experimental data are needed to determine which assumption is most appropriate. For the purposes of the remaining discussion we will use the assumption resulting in equation (9); the results of both equations are well within a reasonable variation of 10%.

It is noteworthy that ξ in equation (9) is not very sensitive to variations in s^*: a change in s^* of the order of 100% results in a change in ξ that is less than 10%. This is very important because the largest uncertainty, both from the experimental point of view and from the theoretical point of view, lies in the estimation of s^*.

Unfortunately experimental data, against which the above model can be tested, are very limited. Although various researchers have performed experiments, very few experiments are presented in a concise way which allows their use for model calibration and evaluation. In the following subsection we present a comparison between the model prediction and experimental data for the case of negligible surface tension. This limiting case presents a good test for any model, primarily because more experimental data are available (Watanabe et al., 1992), and various alternative model predictions have been investigated in this limit (Bennett and Poulikakos, 1994).

Zero surface tension limit

We investigate here the model predictions in the limit $We \to \infty$, that is when surface tension effects are negligible. For $We \to \infty$ equation (9) reduces to

$$\xi = 0.5 Re^{0.25}. \qquad (13)$$

The exponent of 0.25 is very close to the usually quoted exponent of 0.2 (Bennett and Poulikakos, 1994; Pasandideh-Fard et al., 1998; Watanabe et al., 1992). Direct comparison with the experimental data of (Watanabe et al., 1992) reveals that the above equation results is in much better agreement with experimental data than the SMAC (simplified marker and cell) simulation results of Watanabe et al. predicting

$$\xi = 0.82 Re^{0.2}. \qquad (14)$$

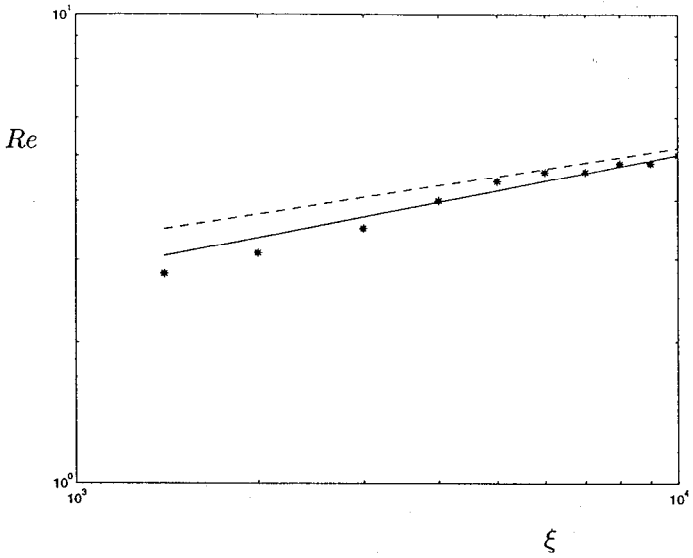

Figure 1. THE SPREAD FACTOR ξ AS A FUNCTION OF THE REYNOLDS NUMBER (Re) IN THE LIMIT $We \to \infty$. THE SOLID LINE REPRESENTS EQUATION (13), THE DASHED LINE REPRESENTS EQUATION (14) AND THE STARS THE EXPERIMENTAL DATA OF WATANABE ET AL.

Further numerical simulations by researchers using the same algorithm (Watanabe et al., 1992) report very similar results ($\xi = 0.83Re^{0.2}$). The Madejski (1976) expression

$$\xi = 1.2941Re^{0.2}, \tag{15}$$

seems to overpredict ξ by a factor of 1.5. The comparison between equations (13), (14), and thc experimental data can be seen in Figure 1.

ESTIMATION OF SOLIDIFIED LAYER THICKNESS

The model developed above makes use of the thickness (s) of the solidified layer in contact with the subcooled target. As discussed by Bennett and Poulikakos (1994), and demonstrated through numerical simulations by Pasandideh-Fard et al. (1998), the Stefan problem approach is inadequate. Pasandideh-Fard et al. show that the more involved calculation that includes the effects of contact resistance and substrate temperature can yield fairly accurate results. We present here an alternative and significantly less cumbersome approach to the estimation of this thickness. This approach was chosen because it is the natural extension of the stagnation flow model used for the evaluation of the flow properties of the spreading droplet, and it also lends itself naturally to the estimation of an average (over the splat diameter) thickness. The approach neglects the effects of varying substrate temperature.

We assume that the Stefan number based on the superheat and the melting point is small, that is $c_p(T_0 - T_m)/h_{fg} \ll 1$. This assumption allows us to set the liquid temperature to the melting point temperature T_m and neglect the energy required to cool the superheated drop to this temperature. Equating the energy lost through contact with the substrate to the change in total energy of the solidified part of the drop we obtain:

$$\frac{\pi D_m^2}{4} s\rho_s(h_{fg} + c_p(T - T_w)) = \frac{1}{2}\frac{\pi D_m^2}{4} h_t(T_m - T_w)\tau. \tag{16}$$

The factor of $1/2$ on the right hand side represents the time average of the area available for heat exchange: the velocity with which the droplet spreads is $u \sim \frac{1}{r}$ and hence the area increase rate is linear with time $dA = 2\pi r dr \sim 2\pi u dt$. The final temperature of the solidified layer is an unknown and introduces some uncertainty in our calculation; this issue is further discussed below. The time $\tau = 8D_0/3V_0$ is taken to be the spreading time defined and discussed in the previous section. The total heat transfer coefficient h_t has two contributions:

$$Nu_t = \frac{h_t D_0}{k} = \frac{1}{\frac{1}{Nu_c} + \frac{1}{Nu_f}}. \tag{17}$$

Here $Nu_c = h_c D_0/k$ is the Nusselt number associated with the contact resistance, and $Nu_f = h_f D_0/k$ is the Nusselt number associated with the flow at the stagnation point. The latter can be evaluated (in the $Pr \to 0$, $We \gg 1$ limit) using the correlation for laminar stagnation point flow due to jet impingement on solid targets (Liu et al., 1993)

$$Nu_f = 1.08Re^{0.5}Pr^{0.5}. \tag{18}$$

Note that the thermal resistance associated with the solid layer formed, $1/h_s = \bar{s}/k_s$, is negligible. In the experiments of Pasandideh-Fard et al. (1998), $Nu_s = h_s D_0/k \approx 80$, whereas $Nu_f \approx Nu_c \approx 10$. The above analysis also neglects the effects due to change of the substrate temperature which we feel would be too complex to be incorporated in such a model. Additionally, the encouraging results obtained with the present model suggest that the importance of the substrate temperature variation is small.

Equation (16) leads to

$$s = \frac{4h_t(T_m - T_w)D_0}{3V_0\rho_s h_{fg}(1 + \frac{c_p(T-T_w)}{h_{fg}})}. \tag{19}$$

Temperature T varies between T_m and T_w, and is difficult to evaluate without further assumptions. We define the Stefan number based on this temperature $Ste_T = \frac{c_p(T-T_w)}{h_{fg}}$, such that $0 < Ste_T < Ste$ and equation (19) becomes

$$s^* = \frac{4Nu_t Ste}{3RePr(1+Ste_T)}. \quad (20)$$

When $Ste \ll 1$ it follows that $Ste_T \ll 1$ and the solidified layer temperature has no effect; in the worst case that $Ste \sim 1$, equation (20) provides an upper and lower bound for s^* which differ by at most a factor of 2, which however, as discussed above, result in only 10% uncertainty in ξ.

The above model is used to reproduce the numerical simulation results of Pasandideh-Fard et al. (1998). In these simulations Nu_c=6.8, $Re = 1.2 \times 10^4$, $We = 71$, and $Pr = 0.0073$. For $T_w = 150^oC$ ($Ste = 0.324$) the numerical simulations give $s^* = 0.014$ and equation (20) gives $0.015 < s^* < 0.02$, whereas for $T_w = 25^oC$ ($Ste = 0.774$) the numerical simulations give $s^* = 0.035$ and equation (20) gives $0.027 < s^* < 0.047$.

CONCLUSIONS

We have developed a model for the approximate calculation of the maximum splat diameter resulting form a superheated liquid metal droplet impacting a subcooled flat surface. The model originates in the work of Pasandideh-Fard et al. (1996, 1998) that successfully addressed the isothermal case; the current work re-addresses the issue of the effect of solidification on the splat diameter that we feel would benefit from an improved representation. The model accounts for the effects of surface tension, viscous dissipation, and contact angle. Good agreement with experimental results available is obtained.

A simple method to estimate the solidified layer thickness that allows for the importance of thermal contact resistance between the substrate and the liquid droplet is also proposed. Comparison with numerical simulations reveals good agreement, making it a preferable method compared to numerical simulations or more involved analytical methods. More thorough tests are required for both models, since the experimental data available to the author are limited.

ACKNOWLEDGMENT

The author would like to thank A. Shapiro for bringing this problem to his attention. This work was perfomed under the auspices of the U.S. Department of Energy under contract W-7405-ENG-48.

REFERENCES

Bennett, T., Poulikakos, D. Splat-quench solidification: estimating the maximum spreading of a droplet impacting a solid surface. Journal of Material Science 1993;28:963-970.

Collings, E.W., Markworth, A.J., McCoy, J.K., Saunders, J.H. Splat-quench solidification of freely falling liquid-metal drops by impact on a planar substrate. Journal of Material Science 1990;25:3677-3682.

Liu, X., Gabour, L.A., Lienhard V, J.H. Stagnation point heat-transfer during impingement of laminar liquid jets: analysis including surface tension. Journal of Heat Transfer 1993;115:99-105..

Madejski, J. Solidification of droplets on a cold surface. International Journal of Heat and Mass Transfer 1976;19:1009-1013.

Pasandideh-Fard, M., Qiao, Y.M., Chandra, S., Mostaghimi, J. Capillary effects during droplet impact on a solid surface. Physics of Fluids 1996;8:650-659.

Pasandideh-Fard, M., Bhola, R., Chandra, S., Mostaghimi, J. Deposition of tin droplets on a steel plate: simulations and experiments. International Journal of Heat and Mass Transfer 1998;41:2929-2945.

Watanabe, T., Kuribayashi, I., Honda, T., Kanzawa, A. Deformation and solidification of a droplet on a cold substrate. Chemical Engineering Science 1992;47:3059-3065.

AN ACCURACY EVALUATION FOR THE MADEJSKI SPLAT-QUENCH SOLIDIFICATION MODEL

Salvador M. Aceves, Arthur B. Shapiro, and Vivek Sahai
Lawrence Livermore National Laboratory

ABSTRACT

Development of methods to spray form materials by precisely controlled deposition of droplets can result in new manufacturing processes which offer improved metallurgical performance and reduced production costs. These processes require a more detailed knowledge of the fluid mechanics, heat transfer and solidification that occur during droplet spreading. Previous work using computer simulations of this process have been difficult to implement and have required long running times. This paper examines the use of an alternative, simplified, method developed by Madjeski for solving for the problem of droplet spreading and solidification. These simplifications reduce the overall splat spreading and solidification problem to a closed-form differential equation. This differential equation is then solved under various conditions as reported from recent publications of experimental and numerical results of drop analysis. The results from the model are compared in terms of maximum splat diameter, minimum splat thickness, and time for the droplet spreading to reach 95% of the maximum diameter. The results indicate that the accuracy of the model can be improved by accounting for energy losses in the initial rate of droplet spreading. The model results show that the predictions of experimental results are improved to within 30% over a wide range of conditions.

NOMENCLATURE

- a solid phase thermal diffusivity
- b thickness of the liquid layer
- d splat diameter
- d^* non-dimensional splat diameter, d/D
- D initial droplet diameter
- e ratio of droplet energy after impact to energy before impact
- k freezing parameter, Equation (2)
- Pe Peclet number, wD/a
- R cylinder radius
- R_o initial cylinder ratio
- Re Reynolds number, $wD\rho/\mu$
- t time
- t^* non-dimensional time, tw/D
- U constant in Equation (3)
- w droplet speed before impact
- We Weber number, $\rho Dw^2/\sigma$
- y solid layer thickness
- z splat height
- z^* non-dimensional splat height, z/D
- ε ratio R_o/D
- ρ_l liquid phase density
- ρ_s solid phase density
- σ surface tension

INTRODUCTION

The problem of liquid droplets impinging on a solid surface has practical applications to multiple processes such as spray cooling, spray forming, microfabrication, microcasting, ink jet technology, and precision solder droplet dispensing. An improved control of these processes requires a more detailed knowledge of the fluid mechanics, heat transfer and solidification that occur during droplet spreading.

The process of droplet spreading and solidification is difficult to analyze due to the effect of multiple factors, including inertia, viscosity, gravity, surface tension, wetting, heat transfer (mainly by conduction and radiation), solidification (possibly under non-equilibrium conditions, Kang et al., 1995), phase transitions in the solid phase (Amon et al., 1996), and interactions with other droplets (Kang et al., 1994).

Some numerical analyses of the process of droplet spreading have been presented to date (Trapaga and Szekely, 1991; Trapaga et al., 1992; Fukai et al., 1993; Fukai et al., 1995; Waldvogel et al., 1996; Zhao et al., 1996; Waldvogel and Poulikakos, 1997; Pasandideh-Fard et al., 1998). These solve for the continuity equation, for the Navier-Stokes equations, and for the energy equation in the liquid and solid phases (and ideally in the substrate too). The solution of these equations is complicated by the presence of phenomena such as a free surface, conduction heat transfer through a contact resistance, a rapidly deforming geometry with a big aspect ratio, and liquid-solid and solid-solid phase transitions. As a result, computer simulations have been difficult to implement and have required long running times.

An alternative, simplified, method for solving for the problem of droplet spreading and solidification has been presented by Madejski (1976). This method uses an overall energy balance for the droplet. The initial kinetic energy of the droplet is converted into potential (surface) energy, or is dissipated due to viscous effects as the droplet spreads. The balance between kinetic, potential and dissipated energy

determines the rate of droplet spreading. Solidification may result due to contact with a cold substrate.

Madejski's method uses a series of simplifications to reduce the overall splat spreading and solidification problem to a closed-form differential equation. The main assumptions are:

1. The droplet transforms instantly from a sphere into a cylinder when it impacts the substrate. No energy is dissipated during this initial transformation of the droplet.
2. The Navier-Stokes equations are not solved. Instead, a velocity field is assumed. The velocity profile selected is a simple velocity field that satisfies the continuity equation.
3. The droplet superheat disappears instantly when the droplet touches the substrate. Contact between the droplet and the substrate is assumed to be perfect (infinite contact heat transfer coefficient).
4. For cases that consider freezing, it is assumed that the solidification starts immediately after impingement. The solid layer thickness at any radial position is proportional to the square root of the time elapsed since the moment in which the droplet touched that radial position. The proportionality constant is calculated from a solution to the Stefan problem for a semi-infinite medium (Carslaw and Jaeger, 1990).
5. The liquid (unfrozen) phase has a thickness that is a function of time, but not a function of position along the splat.
6. The effect of surface wetting and contact angles is neglected.
7. Droplets do not break up when they collide with the substrate.

Madejski's method takes into account three of the most important effects in droplet spreading: viscous dissipation, surface tension, and freezing. This results in a very complete method, considering the simplicity of the analysis. However, many important effects are not considered. These include droplet superheat, thermal contact resistance (Liu et al., 1995), substrate melting, droplet recoil (Fukai et al., 1993), and wetting effects (Fukai et al., 1995).

Some improvements on Madejski's method have been published in the literature. Markworth and Saunders (1992) developed an improved velocity field for application to Madejski's method. The velocity field is improved because it not only satisfies the continuity equation. It also satisfies the appropriate no stress boundary condition at the free surface. The new velocity field can be used to derive new versions of Madejski's equations. Rangel and Bian (1997) have published the resulting equations. Rangel and Bian (1997) have also extended Madejski's method by using the full energy equation and an energy balance to track the solid-liquid interface. The extended method can therefore take into account droplet superheat and substrate melting. Thermal contact resistance could also be implemented in the model.

The main advantage of Madejski's method is its closed form, which is very simple to use. Only three non-dimensional parameters (the Reynolds number, Re; the Weber number, We; and a freezing parameter, k) are enough to determine droplet spreading with Madejski's method. In contrast, detailed numerical analyses of the droplet spreading and solidification require a major effort for implementation and long computer run times. Detailed numerical solutions may also be subjected to limitations in accuracy, due to an inappropriate knowledge of the wetting and heat transfer interactions between the droplet and the substrate. These factors are recognized to be very important in the process of droplet spreading, and obtaining real data for practical applications is a challenge (Pasandideh-Fard et al., 1998).

While a detailed analysis is necessary in many cases, it is important to determine the accuracy of Madejski's model as compared to existing experimental and numerical data. This comparison may help in determine under which regimes Madejski's model gives the best results, and under which regimes it may be used at least as a preliminary tool in determining droplet spreading parameters.

This paper presents a comparison of the results obtained with Madejski's model and those obtained in recent publications, both experimental and numerical. Three magnitudes are compared: maximum splat diameter, minimum splat thickness, and time for droplet spreading to 95% of the maximum diameter.

ANALYSIS

This work uses Madejski's (1976) method with the improved velocity profile presented by Markworth and Saunders (1992). The Schwarz solution (Carslaw and Jaeger, 1990) is used instead of the Neumann solution to predict the freezing rate, according to the recommendation of Rangel and Bian (1997). The full energy equations applied in the solution of Rangel and Bian are not used in this work.

An additional modification to Madejski's method is done beyond those discussed in the previous paragraph. Madejski (1976) defines the parameter ε as $\varepsilon \equiv R_o/D$, where D is the droplet diameter before impact and R_o is the initial radius of the cylinder immediately after impact (it is assumed that the spherical droplet becomes a cylinder immediately upon impact; see Assumption 1 in the Introduction). Madejski originally used $\varepsilon=0.5$. Rangel and Bian later used $\varepsilon=0.74$, which satisfies the equation of conservation of potential energy. However, using $\varepsilon=0.74$ results in considerable instantaneous spreading of the droplet upon impact. Conservation of mass indicates that, for $\varepsilon=0.74$, the height of the cylinder immediately after impact, b, is only 30% of the droplet diameter before impact. This results in a very short time for completion of droplet spreading under many conditions.

In this work, $\varepsilon=0.408$ is used. This results in an initial cylinder height b=D, and a much improved prediction of the time for droplet spreading. Potential energy is not conserved during the impact. However, total energy (kinetic+potential) can still be conserved if the equation for the initial speed of droplet spreading (Equation (16) in Rangel and Bian, 1997) is modified appropriately. The new version of this equation is:

$$\left[\frac{dR}{dt}\right]_{t=0} = w\sqrt{\frac{\frac{5}{3}+\frac{20}{We}\left(1-\varepsilon^2-\frac{1}{3\varepsilon}\right)}{1+\frac{11}{252\varepsilon^6}}} \qquad (1)$$

where We is the Weber number, defined as $We \equiv \rho_l D w^2/\sigma$, w is the droplet velocity before impact, ρ_l is the liquid density and σ is surface tension. The non-dimensional freezing parameter k is defined as (Madejski, 1976):

$$k \equiv 6\varepsilon^2 U \frac{\rho_s}{\rho_l}\sqrt{\frac{\varepsilon}{Pe}} \qquad (2)$$

where Pe is the Peclet number, defined as Pe≡wD/a, a is the thermal diffussivity of the solid layer, and U is the proportionality constant in the solid layer thickness equation, obtained from the solution to the Schwarz problem (Carslaw and Jaeger, 1990).

$$y = U\sqrt{a\,t} \qquad (3)$$

Madejski's equations are solved with Euler's method for solving the differential equation. The integral equation that determines the thickness of the solid layer is solved with Simpson's rule. The program was tested for time step size sensitivity by halving the time step until a negligible change in the solution was obtained. Typical running time is of the order of 1 minute in a current engineering workstation.

RESULTS

A survey of the recent literature on splat formation was conducted, and multiple experimental and numerical results were collected from the available papers. Results were collected for maximum splat diameter, minimum splat thickness, and time for reaching 95% of the maximum diameter. The time for 95% of the maximum diameter is used because this is much easier to determine than the time for reaching the maximum diameter (Fukai et al., 1995).

The conditions and the results found in the references are converted to non-dimensional parameters (Re, We, k, $d^*=d/D$, $z^*=z/D$, and $t^*=tw/D$). A summary of all the information collected from the references is included in Table 1. Much of the information was collected from figures, and it is therefore subjected to reading errors, especially in the case of the splat thickness, due to the small values frequently obtained for it. Some of the spaces are empty because these values were not reported in the references.

Detailed analyses and experiments often show droplet recoil due to surface tension effects, especially for low Weber numbers. Madejski's model does not predict droplet recoil. For this reason, the splat properties listed in Table 1 do not represent final, equilibrium splat conditions. Instead, they represent values at the end of the first splat expansion cycle, before recoil starts. No comparison between Madejski's method and detailed models is possible after the recoil process starts.

Most of the data found in the literature are obtained for isothermal droplet spreading, at conditions for which no freezing occurs. A few cases with freezing are also reported. The literature survey used for this report is by no means exhaustive, but the data cover a wide range of Reynolds and Weber numbers, and should give a good indication of the accuracy of Madejski's method under multiple regimes.

Figure 1 shows non-dimensional maximum droplet diameter (d^*) as a function of Reynolds number and Weber number. The figure shows all the points listed in Table 1, with the original reference identified by symbols. The numbers located next to the symbols indicate the maximum splat diameter obtained from the references. A range of values is given for points that originate from a single reference and are located very close to each other in the figure (data from Fukai et al., 1995, and from Pasandideh-Fard et al., 1998). The figure shows the wide ranges of Reynolds (10^2-10^6) and Weber (1-10^4) numbers studied in the literature.

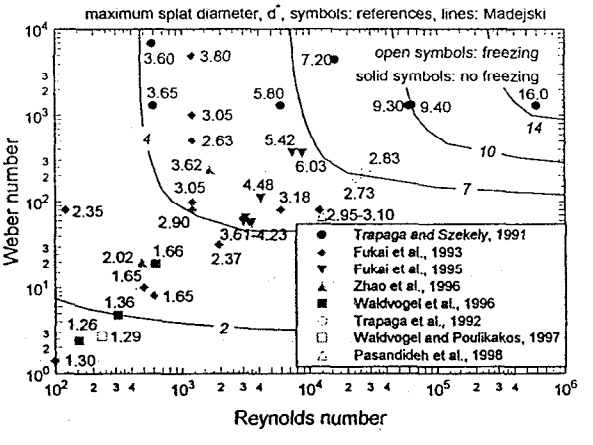

Figure 1. Non-dimensional maximum droplet diameter (d^*) as a function of Reynolds number and Weber number. The figure shows all the points listed in Table 1, with the original reference identified by symbols. The numbers located next to the symbols indicate the maximum splat diameter obtained from the references. The lines in the figure show contours of constant maximum splat diameter, calculated by Madejski's model assuming no freezing conditions (k=0).

The lines in the figure show contours of constant maximum splat diameter, calculated by Madejski's model, assuming no freezing conditions (k=0). Both the lines and the symbols show that the maximum splat diameter tends to grow as the Reynolds and the Weber numbers increase. Some anomalous results are easily identified in the figure. These include the values reported by Zhao et al., 1996, which appear high compared to the values for nearby points reported in other references. This may be due

to effects, such as surface wetting, which cannot be described in terms of the Reynolds and the Weber numbers alone. Another effect not properly described by the Reynolds and the Weber numbers is freezing, and the points with freezing (open symbols in the figure) have maximum diameters that are lower than the neighboring points with no freezing.

Figure 1 indicates that there is good qualitative agreement between Madejski's method and the existing literature. Figure 2 is included to facilitate a quantitative comparison between the references and Madejski's model. Figure 2 shows the ratio of the maximum droplet diameter calculated from Madejski's model and the maximum droplet diameter reported in the references. The figure shows that Madejski's model tends to overestimate the maximum splat diameter. Figure 2 shows that the best agreement is obtained for the data of Trapaga and Szekely (1992) and for the data of Fukai et al. (1995). The agreement improves as the Reynolds and Weber numbers increase. The results for the freezing cases are also overestimated by 30-60%.

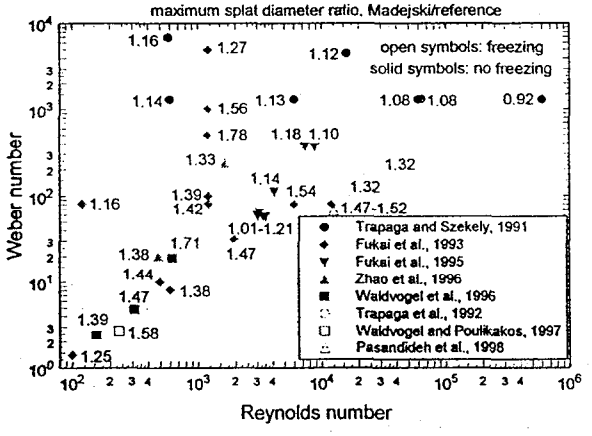

Figure 2. Ratio of the maximum droplet diameter calculated from Madejski's model and the maximum droplet diameter reported in the references as a function of Reynolds number and Weber number. The figure shows all the points listed in Table 1, with the original reference identified by symbols.

Figure 3 shows the ratio of the minimum splat thickness calculated by Madejski's model and the minimum splat thickness as reported in the references. Some points in the figure do not include a number because the minimum splat thickness is not reported in these references. The figure indicates that Madejski's model underestimates the minimum splat thickness in almost all cases. This is consistent with the overestimation of the splat diameter shown in Figure 2, since a bigger splat is necessarily thinner. The relative error in using Madejski's model for predicting splat thickness is greater than the relative error in predicting the splat diameter (Figure 2). This is due in part to the difficulty of reading the small values of the splat thickness from plots presented in the references.

Figure 4 shows the ratio of the time for reaching 95% of the maximum splat diameter calculated by Madejski's model and the time for reaching 95% of the maximum splat diameter reported in the literature. Unlike figures 2 and 3, this figure does not show a definite trend. Madejski's model underpredicts the time for some points and overpredicts the time for some other points. The trend seems to depend more on the original reference than on the location on the Reynolds-Weber plane. Spreading time is underestimated when compared with the results of Trapaga and Szekely (1991), but it is overestimated when compared to those of Fukai et al., (1993). Very good agreement is once more obtained with the results of Fukai et al. (1995).

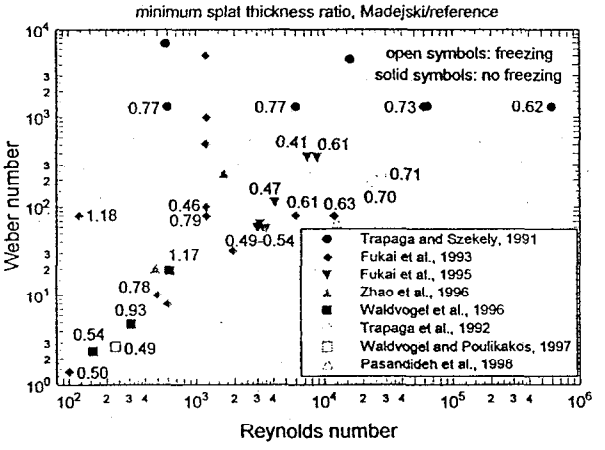

Figure 3. Ratio of the minimum splat thickness calculated from Madejski's model and the minimum splat thickness reported in the references as a function of Reynolds number and Weber number. The figure shows all the points listed in Table 1, with the original reference identified by symbols.

Figures 5 through 7 show a comparison of the splat spreading as a function of time between Madejski's model and some of the references. Figure 5 shows the spreading process for splats at the conditions studied by Trapaga and Szekely (1991). The figure shows the results of Trapaga and Szekely with solid lines and the results of Madejski's method with dotted lines. Madejski's method underpredicts the initial slope of the lines, but the slope then remains fairly constant for a long period of time, resulting in final diameters that closely predict those of Trapaga and Szekely. The lines from Trapaga and Szekely have slopes that drop rapidly. This is due to substantial viscous dissipation in the early stages of the spreading process. In contrast, Madejski's method assumes that no energy losses occur in the initial spreading of the droplet.

Figure 6 shows a comparison of the results of Madejski's model with those of Waldvogel et al. (1996). The figure shows the results of Waldvogel et al. with solid lines and the results of Madejski's method with dotted lines. Figure 2 shows that the

conditions used by Waldvogel et al. (low Reynolds and Weber number) result in a poor agreement with Madejski's model. Figure 6 shows that Waldvogel et al. report substantial droplet recoil, down to diameters lower than the original droplet diameter in some cases. As previously discussed, Madejski's model does not predict droplet recoil in its current form. Droplet solidification should reduce the amount of droplet recoil and improve the accuracy of Madejski's model for low Reynolds and Weber number cases. Figure 6 shows once more that Madejski's model underpredicts the initial rate of viscous energy dissipation. As a consequence, the slopes of the lines remain constant for a long time compared to those of Waldvogel et al.

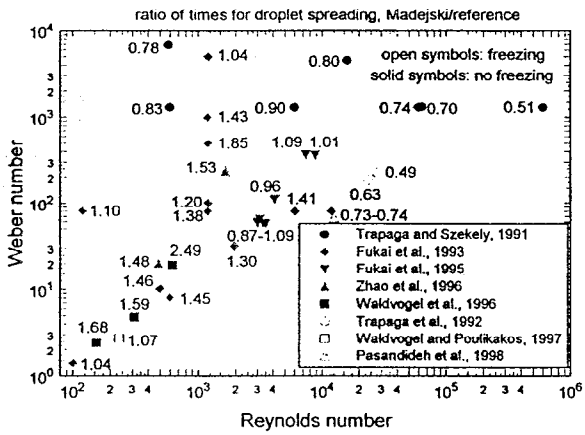

Figure 4. Ratio of the time for reaching 95% of the maximum splat diameter calculated by Madejski's model and the time for reaching 95% of the maximum splat diameter reported in the literature as a function of Reynolds number and Weber number. The figure shows all the points listed in Table 1, with the original reference identified by symbols.

Figure 7 shows a comparison of the results of Madejski's model with those of Pasandideh-Fard et al. (1998). The figures show the results of Pasandideh-Fard et al. with solid lines and the results of Madejski's method with dotted lines. The results of Pasandideh-Fard et al. presented in the figure include the effect of freezing. Some droplet recoil is observed in the results of Pasandideh-Fard et al., although the magnitude of the recoil is much smaller than observed by Waldvogel et al. (1996) shown in Figure 6, partly due to the higher Reynolds number and partly due to freezing. Figure 7 shows that Madejski's model predicts the freezing time reasonably well. This is due in part to the use of near zero initial droplet superheat by Pasandideh-Fard et al. As previously discussed, Madejski's freezing model neglects superheat. The effect of droplet superheat could be estimated and incorporated in Madejski's model, as previously shown by Rangel and Bian (1997).

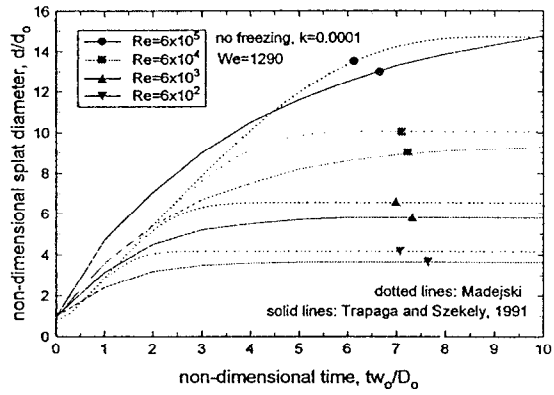

Figure 5. Comparison of the results of Madejski's model and the results of Trapaga and Szekely (1991). The figure shows splat diameter during the spreading process as a function of time. The results of Trapaga and Szekely are shown with solid lines and the results of Madejski's method with dotted lines.

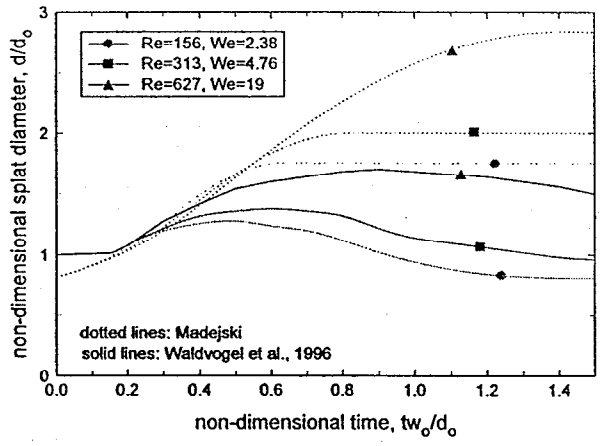

Figure 6. Comparison of the results of Madejski's model and the results of Waldvogel et al. (1996). The figure shows splat diameter during the spreading process as a function of time. The results of Waldvogel et al. are shown with solid lines and the results of Madejski's method with dotted lines.

The previous figures indicate that Madejski's model overpredicts the splat diameter, and as a consequence it underpredicts the splat thickness. This is due in part to the assumption that the droplet turns into a cylinder immediately upon impact with no energy losses in the process. More detailed analyses (Trapaga and Szekely, 1991) indicate that there is substantial energy dissipation in the early stages of splat spreading. Including some energy losses in Madejski's model is

certain to result in better predictions. Energy losses in the initial stage of splat spreading can be included in Madejski's model by modifying the initial rate of droplet spreading (Equation 1). The new form of this equation is:

$$\left[\frac{dR}{dt}\right]_{t=0} = w\sqrt{\frac{\frac{5e}{3}+\frac{20}{We}\left(e-\varepsilon^2-\frac{1}{3\varepsilon}\right)}{1+\frac{11}{252\varepsilon^6}}} \qquad (4)$$

The rest of the formulation is not changed. In Equation (4), e is defined as the ratio of the cylinder energy immediately after impact to the droplet energy before impact. The parameter e was varied in the range $0.1<e<1.0$, and the best agreement with published results was obtained with e=0.6. This value is in reasonably good agreement with the viscous energy dissipation calculated by Trapaga and Szekely (1991) during the initial impact process.

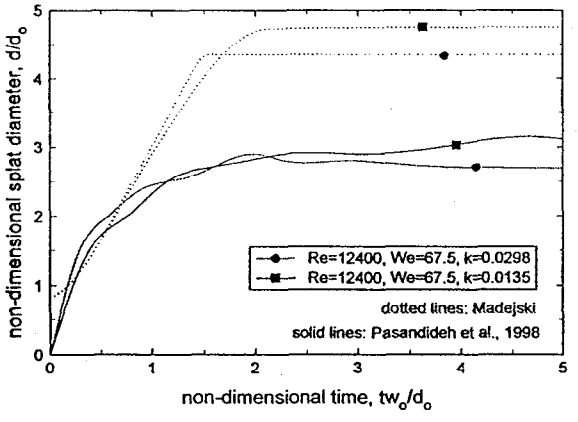

Figure 7. Comparison of the results of Madejski's model and the results of Pasandideh-Fard et al. (1998). The figure shows splat diameter during the spreading process as a function of time. The results of Pasandideh-Fard et al. are shown with solid lines and the results of Madejski's method with dotted lines.

Low values of e combined with low values of We may result in negative values inside the radical in Equation (4), which results in a non-physical, imaginary, number for the initial rate of droplet expansion. For e=0.6, the radical turns negative for points with We<7.7, which includes 4 points in Table 1 and in Figures 2, 3 and 4. For these points the method cannot be applied, and a higher value of e (0.9) has been used for comparison with the results from the references.

The results of the analysis for e=0.6 are shown in Figure 8. Figure 8 shows the same information as Figure 2, with the only difference that the Madejski calculations are done with e=0.6 (e=0.9 for We<7.7). Figure 8 shows the ratio of the maximum droplet diameter calculated from Madejski's model with e=0.6 and the maximum droplet diameter reported in the references. The figure shows a much-improved agreement between Madejski's model and the original references, compared with Figure 2. Almost all the results, including the results for the cases that include freezing, fall within 30% of the values given in the references, and in most cases the agreement is much better throughout the ranges of Reynolds and Weber numbers. This figure indicates that it is necessary to incorporate the initial diffusion of energy in Madejski's model to obtain results that are broadly applicable.

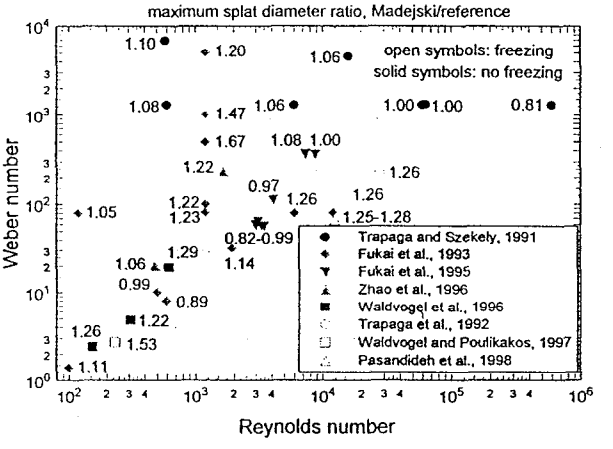

Figure 8. Ratio of the maximum droplet diameter calculated from Madejski's model and the maximum droplet diameter reported in the references as a function of Reynolds number and Weber number. Madejski's model uses an energy ratio e=0.6, except for points with We<7.7, for which e=0.9 is used. The figure shows all the points listed in Table 1, with the original reference identified by symbols.

CONCLUSIONS

This paper uses a modified Madejski's model for calculating droplet spreading and solidification upon impingement on a solid surface. Madejski's model is modified by including an improved velocity profile, the Schwarz solution to predict the freezing rate, a modified aspect ratio for the cylinder formed upon impingement, and a different initial speed of droplet spreading. The results are compared to data published in the recent literature over a Reynolds number range of 10^2 to 10^6 and a Weber number range of 1 to 10^4. Three magnitudes are compared: maximum splat diameter, minimum splat thickness, and time for droplet spreading to 95% of the maximum diameter.

The results show that Madejski's model overpredicts the maximum droplet diameter and underpredicts the minimum splat thickness. No clear trend was found for the predictions of spreading time. Examination of the results shows that the

overprediction of the maximum diameter occurs partly because Madejski's model neglects energy losses in the initial stages of the spreading process. These energy losses result from viscous dissipation. Madejski's model is then modified to take into account these losses by changing the initial rate of droplet spreading. The new results show improved agreement with the maximum splat diameters (within 30% for almost all cases). These results indicate that the modified Madejski's model of droplet spreading presented in this paper can be used to give reasonable predictions of maximum droplet diameter and minimum splat thickness.

ACKNOWLEDGMENTS

This work performed under the auspices of the U.S. Department of Energy by the Lawrence Livermore National Laboratory under Contract W-7405-ENG-48.

REFERENCES

Amon, C.H., Schumaltz, K.S., Merz, R., Prinz, F.B., 1996, "Numerical and Experimental Investigation of Interface Bonding Via Substrate Remelting of an Impinging Molten Metal Droplet," Journal Of Heat Transfer, Vol. 118, pp. 164-172.

Carslaw, H.S., and Jaeger, J.C., 1990, "Conduction of Heat in Solids," Second Edition, Oxford Science Publications, Clarendon Press, Oxford.

Fukai, J., Zhao, Z., Poulikakos, D., Megaridis, C.M., and Miyatake, O., 1993, "Modeling the Deformation of a Liquid Droplet Impinging Upon a Flat Surface," Physics of Fluids A, Vol. 5, pp. 2588-2599.

Fukai, J., Shiiba, Y., Yamamoto, T., Miyatake, O., Poulikakos, D., Megaridis, C.M., and Zhao, Z., 1995, "Wetting Effects on the Spreading of a Liquid Droplet Colliding with a Flat Surface: Experiment and Modeling," Physics of Fluids A, Vol. 7, pp. 236-247.

Kang, B., Zhao, Z., and Poulikakos, D., 1994, "Solidification of Liquid Metal Droplets Impacting Sequentially on a Solid Surface," Journal Of Heat Transfer, Vol. 116, pp. 436-445.

Kang, B., Waldvogel, J., Poulikakos, D., 1995, "Remelting Phenomena in the Process of Splat Solidification," Journal of Materials Science, Vol. 30, pp. 4912-4925.

Liu, W., Wang, G.X., and Matthys, E.F., 1995, "Thermal Analysis and Measurements for a Molten Metal Drop Impacting on a Substrate: Cooling, Solidification and Heat Transfer Coefficient," International Journal Of Heat And Mass Transfer, Vol. 38, pp. 1387-1395.

Madejski, J., 1976, "Solidification of Droplets on a Cold Surface," International Journal Of Heat And Mass Transfer, Vol. 19, pp. 1009-1013.

Markworth, A.J., and Saunders, J.H., 1992, "An Improved Velocity Field for the Madejski Splat Quench Solidification Model," International Journal Of Heat And Mass Transfer, Vol. 35, pp. 1836-1837.

Pasandideh-Fard, M., Bhola, R., Chandra, S., Mostaghimi, J., 1998, "Deposition of Tin Droplets on a Steel Plate: Simulations and Experiments," International Journal Of Heat And Mass Transfer, Vol. 41, pp. 2929-2945.

Rangel, R.H., and Bian, X., 1997, "Metal-Droplet Deposition Model Including Liquid Deformation and Substrate Remelting," International Journal Of Heat And Mass Transfer, Vol. 40, pp. 2549-2564.

Trapaga, G., and Szekely, J., 1991, "Mathematical Modeling of the Isothermal Impingement of Liquid Droplets in Spraying Processes," Metallurgical Transactions B, Vol. 22B, pp. 901-914.

Trapaga, G., Matthys, E.F., Valencia, J.J., and Szekely, J., 1992, "Fluid Flow, Heat Transfer and Solidification of Molten Metal Droplets Impinging on Substrates: Comparison of Numerical and Experimental Results," Metallurgical Transactions B, Vol. 23B, pp. 701-718.

Waldvogel, J.M., Poulikakos, D., Wallace, D.B., and Marusak, R., 1996, "Transport Phenomena in Picoliter Size Solder Droplet Dispension," Journal Of Heat Transfer, Vol. 118, pp. 148-156.

Waldvogel, J.M., and Poulikakos, D., 1997, "Solidification Phenomena in Picoliter Size Solder Droplet Deposition on a Composite Substrate," International Journal Of Heat And Mass Transfer, Vol. 40, pp. 295-309.

Zhao, Z., Poulikakos, D., and Fukai, J., 1996, "Heat Transfer and Fluid Dynamics During the Collision of a Liquid Droplet on a Substrate: Part I-Modeling," International Journal Of Heat And Mass Transfer, Vol. 39, pp. 2771-2789.

Table 1. Non-dimensional parameters obtained from the literature for the problem of droplet spreading, without and with freezing. The test results are the maximum splat diameter, the minimum splat thickness, and the time to reach 95% of the maximum splat diameter.

Results without freezing	Test conditions			Test results		
Reference	Reynolds	Weber	k	$d^* \equiv d/D$	$z^* \equiv z/D$	$t^* \equiv tw/D$
Trapaga and Szekely, 1991	585	6,800	0	3.60		2.40
	600	1,290	0	3.65	0.05	2.20
	6,000	1,290	0	5.80	0.02	3.20
	16,000	4,500	0	7.20		4.50
	60,000	1,290	0	9.30	0.01	5.95
	63,570	1,304	0	9.40		6.40
	600,000	1,290	0	16.00	0.01	13.00
Fukai et al., 1993	100	1.4	0	1.30	0.50	0.40
	120	80	0	2.35	0.08	1.10
	500	10	0	1.65	0.15	0.60
	600	8	0	1.65		0.55
	1,200	80	0	2.90	0.05	1.25
	1,200	100	0	3.05	0.08	2.00
	1,200	500	0	2.63		1.10
	1,200	1,000	0	3.05		1.45
	1,200	5,000	0	3.80		2.07
	1,944	31.6	0	2.37		1.10
	6,000	80	0	3.18	0.05	1.50
	12,000	80	0		0.04	
Fukai et al., 1995	3,010	58.4	0	4.04		1.90
	3,130	64.1	0	3.61	0.07	1.71
	3,320	57.5	0	3.94		2.08
	3,490	56.8	0	4.23	0.11	2.01
	4,130	111	0	4.48	0.06	2.29
	7,390	364	0	5.42	0.04	2.58
	8,800	359	0	6.03	0.03	2.86
Zhao et al., 1996	485	20	0	2.05		0.95
	1,650	235	0	3.62		1.90
Waldvogel et al., 1996	156	2.38	0	1.26	0.40	0.30
	313	4.76	0	1.36	0.18	0.41
	627	19	0	1.66	0.07	0.57
Results with freezing						
Reference	Reynolds	Weber	k	d/D	z/D	tw/D
Trapaga et al., 1992	23,537	185	0.07	2.73	0.13	1.53
	27,700	223	0.06	2.83	0.12	2.10
Waldvogel and Poulikakos, 1997	235	2.68	0.23	1.29	0.48	0.42
Pasandideh-Fard et al., 1998	12,412	67.5	0.01	3.10		4.19
	12,412	67.5	0.03	2.95		2.13

Droplet Drag and Heat Transfer during Flight

by

Salvador M. Aceves

This report describes the calculations done for predicting droplet speed and temperature at the moment of impact with a metallic substrate, for application to a droplet-based manufacturing project. Figure 1 shows a schematic of the experimental apparatus being used at UC Irvine for this project. The figure also includes many of the relevant dimensions.

The analysis includes the evolution of the droplet as it moves along all the different parts of the apparatus. The analysis for each part is as follows:

1. Droplet Generator

The orifice size in the droplet generator determines the size of the droplet. This analysis considers a 50 μm orifice radius. The frequency of droplet generation and the radius of the droplet are calculate from the following equations (Orme et al., 1996):

$$f = \frac{k_0^* v}{2 \pi r_0} \tag{1}$$

$$r_d = \left(\frac{3}{2} \frac{\pi r_0^3}{k_0^*} \right)^{\frac{1}{3}} \tag{2}$$

In these equations, f is the frequency, k_0^* is the non-dimensional wave number (equal to 0.697 to obtain the most uniform droplet behavior), v is the initial velocity of the jet, r_0 is the orifice radius, and r_d is the droplet radius. The resulting droplet diameter is 189 μm, and the frequency of droplet generation is 20000 droplets/s.

2. Charge Electrode

The charge electrode is installed to charge the droplets being produced. The voltage on the electrode is variable, to direct the droplets to the desired location. The range of voltages used is 0-400 V. The voltage is changed rapidly to charge only one out of every two droplets, to avoid charge interactions between the droplets. The charge in the droplet is calculated from Equation (3) (Schneider et al., 1967).

$$q = \frac{2\,\varepsilon_0\,V_0\,m}{r_0^2\,\rho\,ln(B/r_0)} \qquad (3)$$

In this equation, q is the charge of each droplet, ε_0 is the permittivity constant (ε_0=8.854x10^{-12}C^2/Nm^2), V_0 is the voltage between the plates, m is the mass of the droplet, ρ is the density of the droplet, and B is the radius of the charge electrode.

3. Deflection Plates

These plates are kept at a constant voltage, so that the intensity of the electric field between the plates is constant at E=6x10^5 V/m. Charged droplets are deflected, and uncharged droplets are not. A gutter intercepts uncharged droplets, and this material can be recycled. The force on charged droplets due to the electric field is:

$$F = q\,E \qquad (4)$$

4. Substrate

The droplets collide with a copper substrate to form the part being manufactured. The temperature and speed of the droplet when it collides with the substrate determine the characteristics of the part being made.

5. Environmental Chamber

All the experimental components are located inside an environmental chamber that can be filled with inert gases and pressurized (or depressurized). Nitrogen is normally used as the inert gas, but CO_2 is also considered here, since it may provide some advantages.

Drag Calculation

Droplets are produced with a high frequency, so that the initial distance between droplets is small (450 μm, or 2.38 times the droplet diameter). For this very small distance between droplets, there is a significant reduction in droplet drag caused by the wake of the previous droplet. To calculate drag coefficients under these conditions, Mulholland's correlation is used (Mulholland et al., 1988).

Only half of the droplets are charged and deflected by the deflection plates. The gutter intercepts the other half of the droplets. The remaining droplets are deflected in different directions, so that it is probably safe to assume that droplets do not interact with each other after they fall below the deflection plates. For this reason, a single-droplet drag correlation (Clift et al., 1978) is used for droplets that fall below the deflection plates.

The single-droplet drag equation is:

$$C_D^{\infty} = (24/Re)(1 + b\,Re^{0.687}) \qquad (5)$$

This equation is valid for Re<800.

For droplets that interact with each other, Mulholland's correlation is used. This is expressed by the following set of equations:

$$\left(C_D\right)^{-n} = \left(C_D^{\infty}\right)^{-n} + \left(C_D^{0}\right)^{-n} \tag{6}$$

where C_D^{∞} is given by Equation (5), and:

$$C_D^{0} = C_D^{0'} + a\,Re^{-1}(L/D - 1) \tag{7}$$

$$\left(C_D^{0'}\right)^{-n} = \left(C_{D,rod}\right)^{-n} - \left(C_D^{\infty}\right)^{-n} \tag{8}$$

and $C_{D,rod}$ is the drag on a solid rod, given by:

$$C_{D,rod} = 0.755 / Re \tag{9}$$

In these equations, a, b and n are constants fitted from experimental results, given as: a=43.0±15.4, b=0.11, and n=0.678±0.07. Mulholland et al. (1988) show that the big uncertainty in a has little effect in the drag calculation.

Heat Transfer Calculation

Again, the calculation assumes that droplets are not affected by other droplets once they fall below the deflection plates. In this case, the Nusselt number is calculated from a regular, single-droplet correlation (Whitaker, 1972).

$$Nu_{\infty} \equiv \frac{hd}{k_a} = 2 + (0.4\,Re^{0.5} + 0.06\,Re^{0.67})\,Pr^{0.4}\left(\frac{\mu_{\infty}}{\mu_s}\right)^{0.25} \tag{10}$$

In this equation, Pr is the Prandtl number, μ_{∞} is the viscosity of the gas at the free stream condition, and μ_s is the viscosity of the gas at the temperature of the droplet. All properties other than μ_s are evaluated at the free stream conditions.

For the initial period of droplet fall, the droplets are very much affected by the wake generated by other droplets. A correlation developed by Chiang and Sirignano (1991) is used, although its range of validity is limited (droplet distances between 1.35 and 6 diameters, and Reynolds numbers between 90 and 130). A more general expression would clearly be desirable. Chiang and Sirignano's correlation is:

$$\frac{Nu}{Nu_{\infty}} = 1 - aD_{12}^{\ b}D_{23}^{\ c} \tag{11}$$

In this equation, Nu_∞ is given by Equation (10), D_{12} and D_{23} are the distances from the droplet to the droplet ahead and to the droplet behind in a continuous droplet sequence. Correlations with experimental data yielded a=1.281, b=-0.175 and c=-0.398.

Equations of Motion and Energy Equation

The equations of motion are obtained from Orme et al. (1996). They are as follows:

$$m\frac{dv_x}{dt} = q\,E - \frac{1}{2}C_D\,\rho_a\,v^2\,A_p\,\sin\Theta \qquad (12)$$

$$m\frac{dv_y}{dt} = mg - \frac{1}{2}C_D\,\rho_a\,v^2\,A_p\,\cos\Theta \qquad (13)$$

In these equations, $\sin\Theta=v_x/v$, and $\cos\Theta=v_y/v$, v is the magnitude of the velocity, A_p is the projected area of the droplet, and E, the intensity of the electric field, has a non-zero value only when the droplet is between the deflection plates.

The energy equation is:

$$mc_p\frac{dT}{dt} = hA(T_\infty - T) + \sigma A(T_\infty^4 - T^4)\in \qquad (14)$$

In this equation, A is the surface area of the droplet, σ is the Stefan-Boltzmann constant ($\sigma=5.67\times10^{-8}$ w/m^{2}K^4), and $\in$ is the emissivity of the droplet, assumed equal to 0.04 for aluminum. The equations of motion and energy are solved with an Euler equation solver. The solution was tested for time step sensitivity by halving the time step. This change resulted in a negligible change in the solution. The initial droplet speed is 9 m/s and the initial temperature is 1200 K. The melting temperature of aluminum is 933 K.

Results

The results are presented in Figures 2-9. Figure 2 shows the droplet path (blue line) and the droplet temperature (green line) as a function of droplet vertical position, y. The vertical position is measured from the droplet generator (y=0) to the substrate (y=50 cm). The figure also shows the vertical position of the deflection plates (17 cm to 21 cm down from the droplet generator). The figure is for a droplet falling in CO_2 gas at 1 atmosphere, with maximum (400 V) voltage at the charging electrode. The figure shows that the droplet falls vertically until reaching the deflection plates that accelerate it in the x-direction. The final droplet deflection in the x-direction is 4 cm. The scale in the x-axis is much greater than in the y-axis, so the droplet path is much more vertical than it appears in the figure.

Figure 2 also shows that the temperature drops from the initial value (1200 K) as the droplet falls. The figure shows a sudden change in the slope of the temperature line as the droplet passes by the deflection plates. Above the plates, there is a significant reduction in heat transfer due to interactions between droplets. Below the plates the droplets are assumed to behave as single droplets, resulting in a much higher convection heat transfer rate.

Figures 3 and 4 show droplet superheat in Kelvins at the time of impingement, as a function of voltage in the charge electrode and pressure inside the chamber. Figure 3 shows the results for a droplet falling in nitrogen and Figure 4 for CO_2. The figure shows that droplet superheat at impingement increases as the pressure is reduced. The line marked 0 represents droplets falling at the melting temperature. The superheat when the droplet is generated is 1200 K –933 K=267 K. It is desirable to have some superheat at impingement, to remelt the substrate and produce a good quality part. Therefore, it may be desirable to operate the environmental chamber under a vacuum to minimize heat transfer from the droplets to the gas inside the chamber. The required superheat can be calculated from a thermal model of the substrate. Modeling the substrate in connection to the droplet fall is planned as a future activity.

Figures 3 and 4 indicate that the use of CO_2 gas reduces heat transfer on the droplet. This can be seen from the higher levels of superheat shown in Figure 4 compared to Figure 3, and is the result of the higher density and lower thermal conductivity of CO_2. Based on these results, it is considered that CO_2 may be a better choice for gas inside the environmental chamber.

Figures 5 and 6 show the droplet deflection in the horizontal direction at the moment of impingement, in cm, as a function of the pressure and the charge plate voltage. Figure 5 shows the results for a droplet falling in N_2 gas and Figure 6 for CO_2. The deflection is mainly a function of voltage, and it does not change much with pressure. Maximum deflection is about 4 cm, obtained at maximum voltage and pressure.

Figure 7 shows the droplet velocity at the moment of impingement as a function of pressure inside the environmental chamber, for a 189-micron droplet falling in N_2 and CO_2 gas. The figure shows that the droplet impinges into the substrate with less velocity when the environmental chamber is full of CO_2 gas. Velocity is shown only as a function of pressure because it is a very weak function of charging voltage.

Figures 8 and 9 show the Reynolds and Weber number for the droplet in the moment of impingement, as a function of the pressure inside the environmental chamber, for droplets falling in N_2 and CO_2 gas. The lines in Figure 8 are identical in shape to those in Figure 7, because the Reynolds number is proportional to the droplet velocity. The lines in Figure 9 are slightly different in shape because the Weber number is proportional to the second power of the velocity.

The Reynolds and Weber numbers are plotted because they are the most important parameters for droplet spreading (Madejski, 1976), and should therefore be important in future work when the droplet flight analysis is linked to the substrate analysis.

Both the Reynolds and the Weber numbers tend to grow as the pressure is reduced, and they are both very weak functions of charge voltage. Values of Reynolds and Weber number shown in the figure for low pressure are in a regime that has not received much attention in droplet spreading analysis (Aceves et al., 1999). Madejski's correlation predicts a spread ratio (initial droplet diameter/final splat diameter) of about 2. Reynolds number in Figure 8 is defined in terms of the density of the liquid phase (droplet), in contrast with the Reynolds number used for the drag calculation, which is defined with the density of the gaseous phase.

Conclusions

A model has been developed for analysis of the process of droplet flight from the droplet generator to a substrate. The model takes into account drag, convection and radiation heat transfer, interaction between droplets, and deflection due to electric charge. The model is used for evaluating droplet parameters at the moment of impingement with a substrate. The model is being developed as a tool for analysis of a droplet deposition experiment.

Future Work

The present analysis of drag and heat transfer will be incorporated into a substrate model to analyze the properties of the piece being manufactured as a function of the droplet flight parameters. Orme and Huang (1997) have developed such model, which can be integrated with the current model for analysis and possibly for optimization of the flight parameters, so that the best conditions for manufacture are obtained.

Future work may also include improvements on the current model. The Nusselt correlation for interacting droplets may need improvement. However, a literature survey did not reveal the existence of a correlation that may apply to a general case.

This analysis neglects evaporation of the droplet. However, as the droplet temperature is increased, some of the droplet material may evaporate. It is important to determine a droplet temperature that represents an upper limit to the temperature range at which it can be safely assumed that evaporation does not play a role in this problem.

Nomenclature

a, b, n parameters for drag correlation, Equations (5)-(9)
a, b, c parameters for heat transfer correlation, Equations (10)-(11)
A surface area of droplet
A_p projected area of droplet, $4\pi r_d^2$

B	radius of the charge electrode
C_D	drag coefficient
c_p	specific heat at constant pressure
d	droplet diameter
E	electric field intensity
f	frequency of droplet generation
F	force
h	heat transfer coefficient
k	thermal conductivity
k_o^*	non-dimensional wave number for droplet generator
L	distance between consecutive droplets
m	droplet mass
Nu	Nusselt number based on gas properties
Pr	Prandtl number for the gas
q	electric charge
r_0	radius of droplet generator orifice
r_d	droplet radius
Re	Reynolds number for gas
T	temperature
T_∞	gas temperature far from droplet
v	velocity
V_0	voltage between charging plates
$\in$	emissivity
ε_0	permittivity constant ($\varepsilon_0=8.854\text{x}10^{-12}C^2/Nm^2$)
μ	viscosity of the gas
Θ	angle between the vertical and the velocity vector
ρ	density
σ	Stefan-Boltzmann constant

References

Aceves, S. M., Shapiro, A.B., and Sahai, V., 1999, "An Accuracy Evaluation for the Madejski Splat-Quench Solidification Model," Submitted for Publication, ASME IMECE, Nashville, TN.

Chiang, C.H., and Sirignano, W.A., 1991, "Axisymmetric Calculations of Three-Droplet Interactions," Proceedings of the ICLASS-91 meeting, Gaithersburg, MD, pp. 719-726.

Clift, R., Grace, J.R., and Weber, M.E., 1978, "Bubbles, Drops and Particles," Academic Press, New York, 1978.

Madejski, J., 1976, "Solidification of Droplets on a Cold Surface," International Journal Of Heat And Mass Transfer, Vol. 19, pp. 1009-1013.

Mulholland, J.A., Srivastava, R.K., and Wendt, J.O.L., 1988, "Influence of Droplet Spacing on Drag Coefficient in Nonevaporating, Monodisperse Streams," AIAA Journal, Vol. 26, pp. 1231-1237.

Orme, M. and Huang, C., 1997, "Phase-Change Manipulation for Droplet-Based Solid Freeform Fabrication," Journal of Heat Transfer, Vol. 119, pp. 818-823.

Orme, M., Huang, C., and Courter, J., "Precision Droplet-Based Manufacturing and Material Synthesis: Fluid Dynamics ad Thermal Control Issues," Atomization and Sprays, Vol. 6, pp. 305-329.

Schneider, J.M., Lindblad, N.R., Hendricks, C.D., and Crowley, J.M., 1967, "Stability of an Electrified Liquid Jet," Journal of Applied Physics, Vol. 38, pp. 2599-2605.

Whitaker, S., 1972, "Forced Convection Heat Transfer Correlationsfor Flow in Pipes, Past Flat Plates, Single Cylinders, Single Spheres and Flow in Packed Beds and Tube Bundles," AIChE Journal, Vol. 18, pp. 361-371.

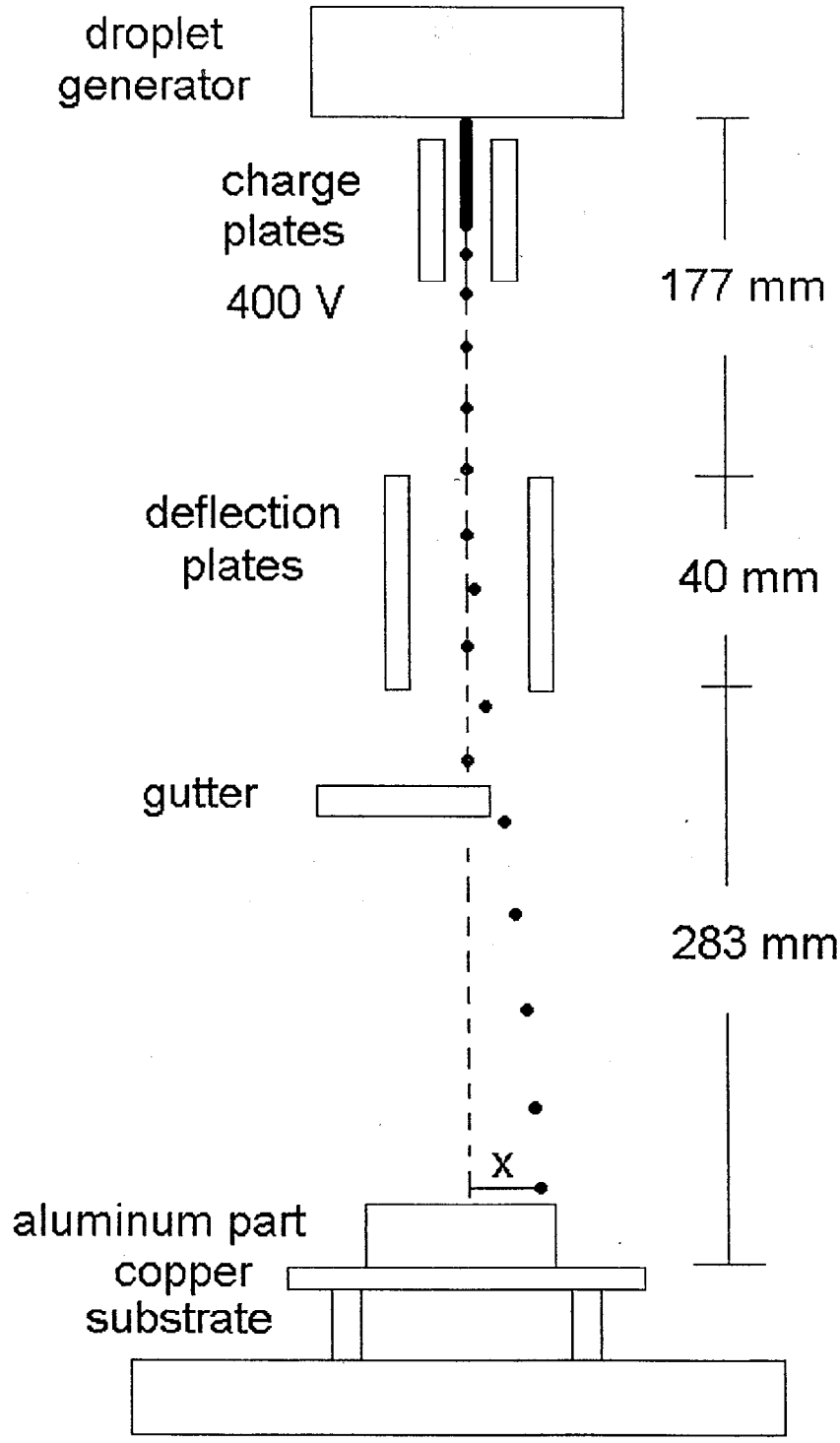

Figure 1. Schematic of the droplet generation and droplet-based manufacturing equipment.

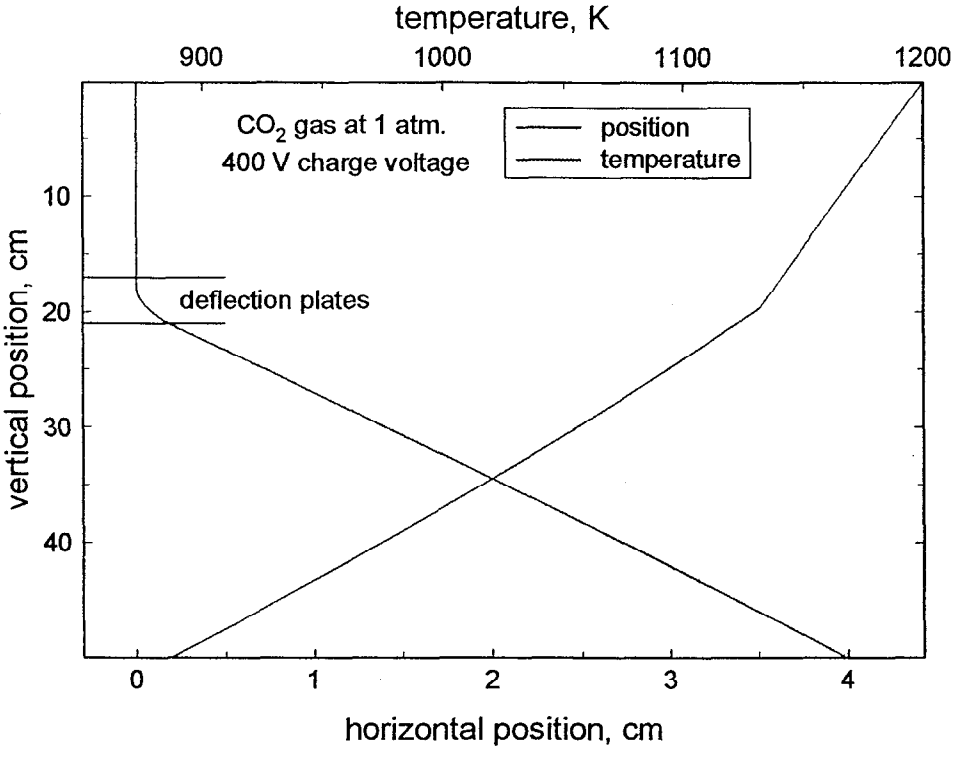

Figure 2. Droplet path (blue line) and droplet temperature (green line) as a function of droplet vertical position, y. The vertical position is measured from the droplet generator (y=0) to the substrate (y=50 cm). The figure also shows the vertical position of the deflection plates (17 cm to 21 cm down from the droplet generator). The figure is for a droplet falling in CO_2 gas at 1 atmosphere, with maximum (400 V) voltage at the charging electrode.

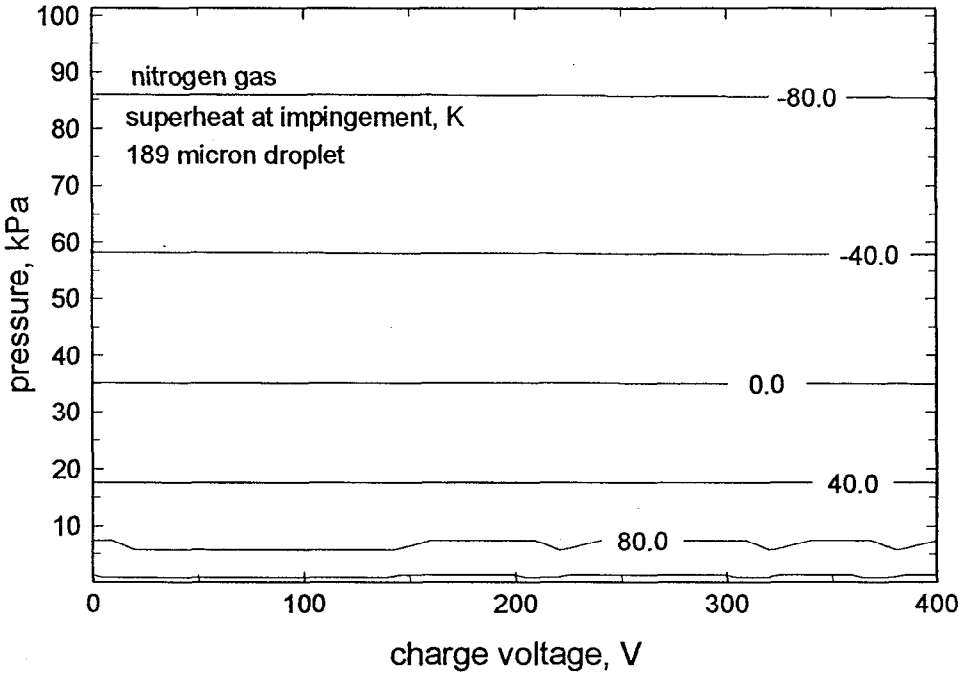

Figure 3. Droplet superheat in Kelvins at the time of impingement, as a function of voltage in the charge electrode and pressure inside the chamber, for a droplet falling in nitrogen.

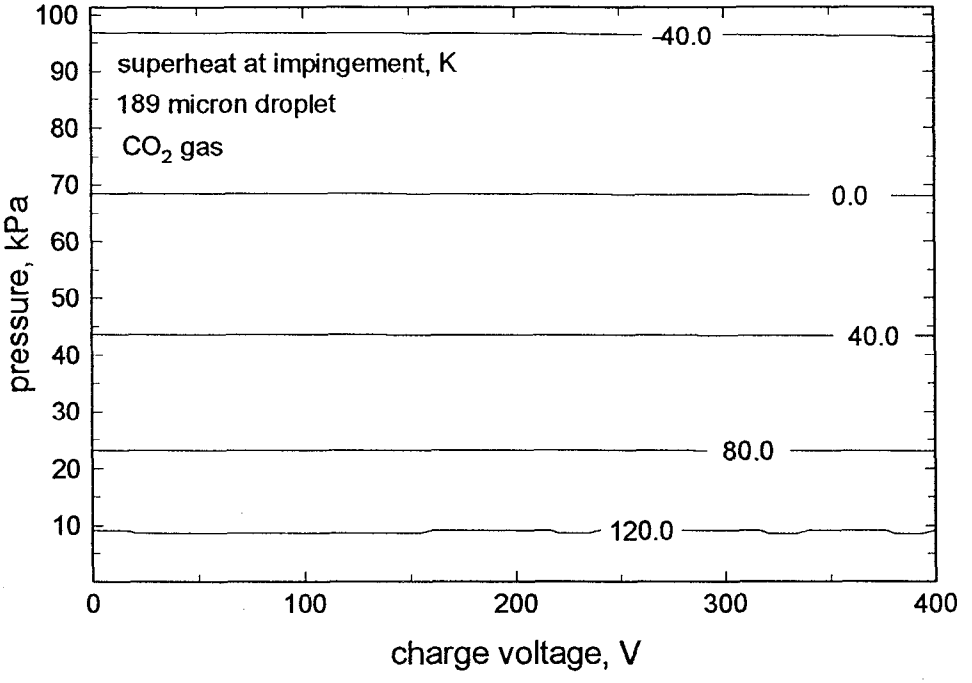

Figure 4. Droplet superheat in Kelvins at the time of impingement, as a function of voltage in the charge electrode and pressure inside the chamber, for a droplet falling in CO_2.

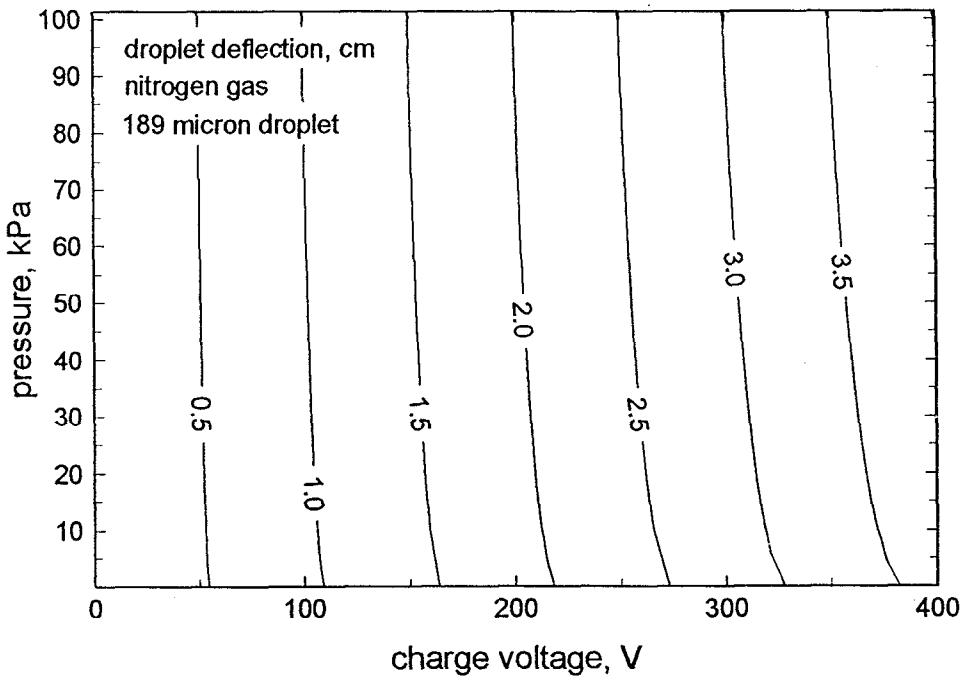

Figure 5. Droplet deflection in the horizontal direction at the moment of impingement, in cm, as a function of the pressure and the charge electrode voltage, for a droplet falling in N_2 gas

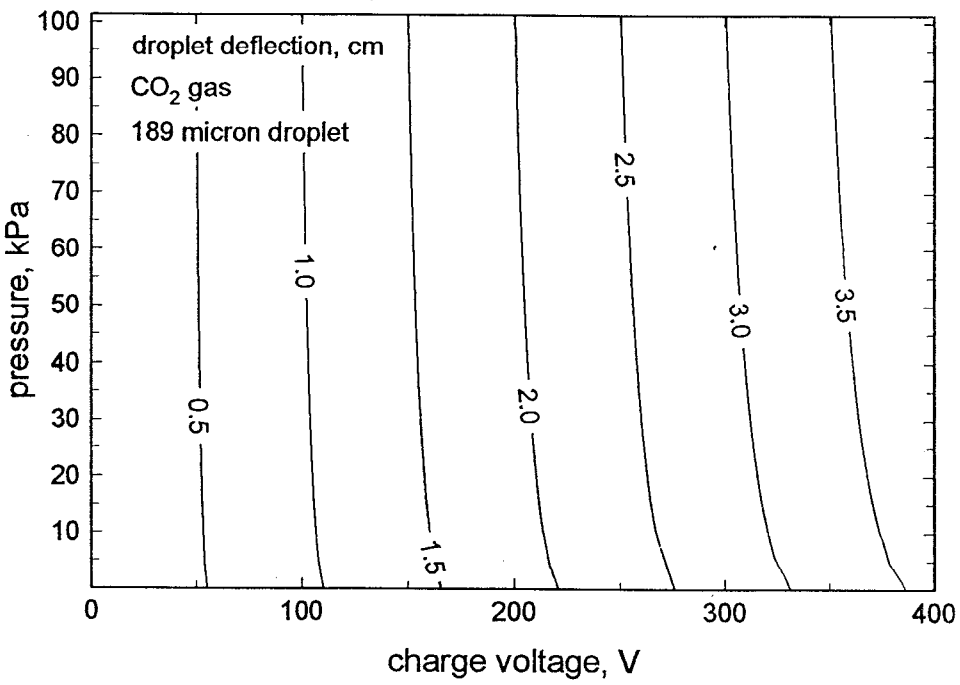

Figure 6. Droplet deflection in the horizontal direction at the moment of impingement, in cm, as a function of the pressure and the charge electrode voltage, for a droplet falling in CO_2 gas

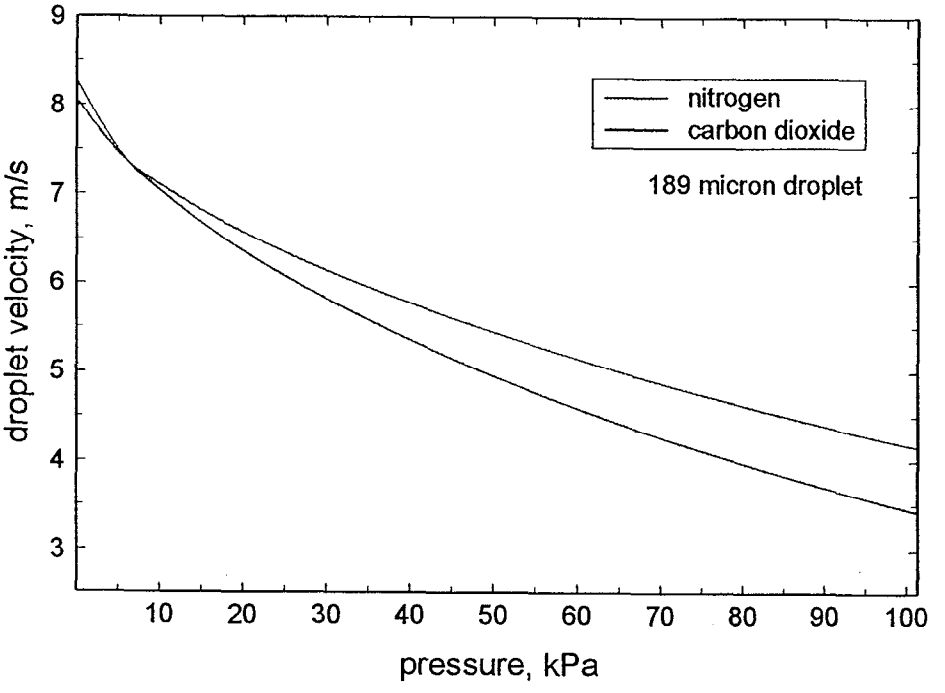

Figure 7. Droplet velocity at the moment of impingement, as a function of pressure, for droplets falling in N_2 and CO_2 gas.

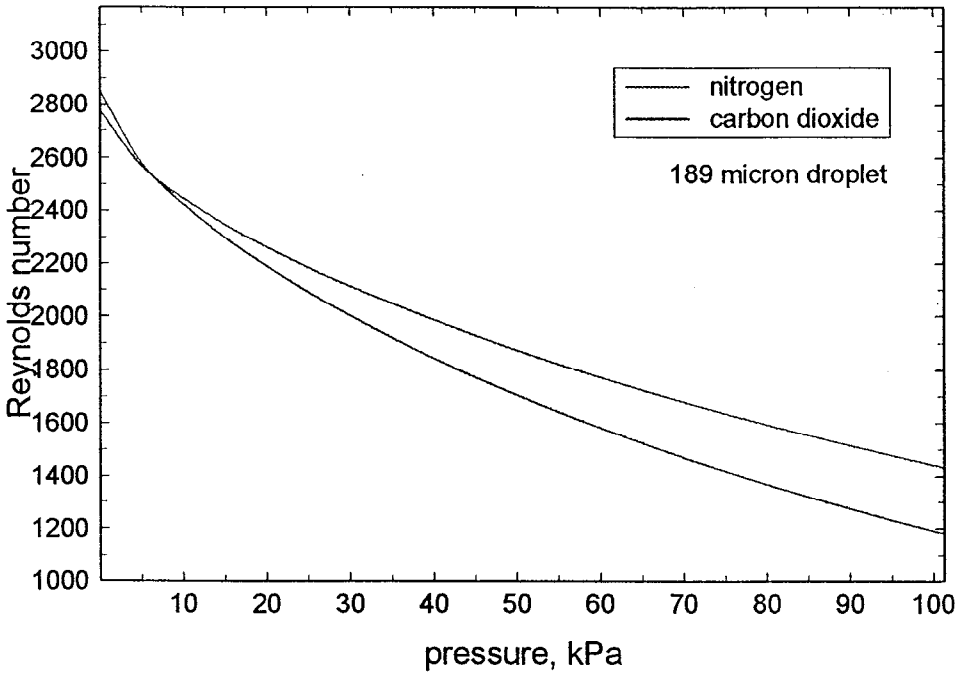

Figure 8. Reynolds number for the droplet in the moment of impingement, as a function of pressure, for droplets falling in N_2 and CO_2 gas.